

The integrated galaxy-wide stellar initial mass function over the radial acceleration range of early-type galaxies

J. Dabringhausen¹, * P. Kroupa^{1,2}

¹ Charles University, Faculty of Mathematics and Physics, Astronomical Institute, V Holešovičkách 2, CZ-180 00 Praha 8, Czech Republic

² Helmholtz-Institut für Strahlen- und Kernphysik, Universität Bonn, Nussallee 14-16, 53115 Bonn, Germany

14 September 2023

ABSTRACT

The observed radial accelerations of 462 Early-type galaxies (ETGs) at their half-mass radii are discussed. They are compared to the baryonic masses of the same galaxies, which are derived from theoretical expectations for their stellar populations and cover a range from $\approx 10^4 M_\odot$ to $\approx 10^{11} M_\odot$. Both quantities are plotted against each other, and it is tested whether they lie (within errors) along theoretical radial acceleration relations (RARs). We choose the Newtonian RAR and two Milgromian, or MONDian RARs. At low radial accelerations (corresponding to low masses), the Newtonian RAR fails without non-baryonic dark matter, but the two MONDian ones may work, provided moderate out-of-equilibrium dynamics in some of the low-mass ETGs. However all three RARs fail at high accelerations (corresponding to high masses) if all ETGs have formed their stellar populations with the canonical stellar initial mass function (IMF). A much better agreement with the observations can however be accomplished, if the theory of the integrated galaxy-wide stellar initial mass functions (IGIMFs) is used instead. This is because the IGIMF-theory predicts the formation of an overabundance of stellar remnants during the lifetime of the massive ETGs. Thus their baryonic masses today are higher than they would be if the ETGs had formed with a canonical IMF. Also the masses of the stellar-mass black holes should be rather high, which would mean that most of them probably formed when the massive ETGs were not as metal-enriched as they are today. The IGIMF-approach confirms downsizing.

Key words: galaxies: dwarf – galaxies: elliptical and lenticular, CD – galaxies: kinematics and dynamics – stars: luminosity function, mass function

1 INTRODUCTION

Mass estimates for galaxies is an active field of research, where a number of surprising and intriguing discoveries have been made.

In spiral galaxies, rotation curves were measured to ever larger distances from the centres of these galaxies. It thereby turned out that the rotation curves flattened out (Rubin et al. 1978; Bosma 1981). This stands in contrast to declining rotation curves at large distances, as the amount of directly observable matter predicts under the assumption of Newtonian dynamics. A straight-forward and popular explanation of this finding is that an additional component of unseen matter alters the potential of spiral galaxies, and thus their rotation curves (Bosma 1981; Rubin et al. 1985). This includes the one of the Milky Way (Bahcall 1984a,b).

Also the dynamics of elliptical galaxies can be inter-

preted as a consequence of unseen matter (Cappellari et al. 2006; Bolton et al. 2008; Tortora et al. 2009). The most extreme known cases are the large number of low-luminosity ETGs that surround the Milky Way, which exhibit optical mass-to-light ratios of up to some 10^3 or even 10^4 in Solar units, if they are assumed to be in virial equilibrium (e.g. Mateo 1998; Strigari et al. 2008; Wolf et al. 2010; Ackermann et al. 2014).

For this reason, the low-luminosity ETGs are often interpreted as representing the most non-baryonic cold dark-matter (CDM) dominated galaxies in the Universe (e.g. Strigari et al. 2008). CDM in general would gather into haloes through gravitational collapse (Navarro et al. 1996; Moore et al. 1998; Gao et al. 2004). Some CDM-haloes are thought to not even contain a galaxy (e.g. Li et al. 2010), while every primordial galaxy would be in a CDM-halo. However, the theory of General Relativity (Einstein 1916) is left unaltered with this approach, which leads eventually to the Λ CDM-model. The Λ CDM-model is summa-

* E-mail: joerg@sirrah.troja.mff.cuni.cz

alized in Planck Collaboration et al. (2020), but also see Del Popolo & Le Delliou (2017), Bullock & Boylan-Kolchin (2017) and Perivolaropoulos & Skara (2021).

Observations imply that low-mass ETGs are indeed very common inside and outside the Local Group (Misgeld et al. 2008, 2009; Javanmardi et al. 2016), while detecting the faintest ETGs, let alone measuring their dynamics, is still a serious observational challenge even in the Local Group. But in any case, the apparently rotationally supported disks of low-mass ETGs around the major galaxies in the Local Group cast serious doubts on the notion that the low-mass ETGs are primordial, CDM-dominated galaxies (Kroupa et al. 2005; Metz & Kroupa 2007; Metz et al. 2008; Pawlowski et al. 2012; Ibata et al. 2013; Hammer et al. 2013; Pawlowski et al. 2013, 2015; Pawlowski & Kroupa 2020; Patel et al. 2020; Pawlowski & Tony Sohn 2021). Disks of satellites are also a frequent feature beyond the Local Group (Ibata et al. 2014, 2015; Müller et al. 2016, 2018, 2021). The reason why they are problematic in the Λ CDM-model is that the Λ CDM-model predicts a predominantly random distribution and motion of such primordial dwarfs around their host galaxies. As an alternative scenario, it has been suggested that low-luminosity ETGs formed out of the matter that was torn out of encountering galaxies through tidal forces, which makes the formation of rotating disks of satellites simply a consequence of the conservation of angular momentum (Kroupa et al. 2005; Kroupa et al. 2010; Pawlowski et al. 2012; Pawlowski et al. 2014; Pawlowski 2018). There is indeed strong evidence that many, if not most low-mass ETGs are tidal dwarf galaxies (e.g. Okazaki & Taniguchi 2000; Kroupa et al. 2010; Dabringhausen & Kroupa 2013). Such tidal dwarf galaxies would however consist almost entirely of baryonic matter, even if their progenitor galaxies contained a substantial amount of CDM (Barnes & Hernquist 1992b; Duc et al. 2004; Bournaud & Duc 2006; Bournaud 2010). Thus, the high internal velocity dispersions of low-luminosity ETGs are likely to have other reasons than a deepening of their potential wells through a presence of CDM.

An alternative approach to postulating the presence of CDM was made by Milgrom (1983b), who augmented the theory of gravitation in the limit of weak gravitational fields, instead of proposing new kinds of matter and energy. This modification is known as Modified Newtonian Dynamics (MOND), or Migromian Dynamics, and is one example of the modified gravity theories. MOND has passed many observational tests, as documented e.g. in the reviews by Famaey & McGaugh (2012) and Banik & Zhao (2021). Recent highlights are the possible detection of the external field effect (EFE) by Haghi et al. (2016); Chae et al. (2020, 2021) and asymmetric tidal tails of open star clusters (Kroupa et al. 2022). The EFE is a phenomenon specific to modified gravity theories, but absent to the Λ CDM-model (Chae 2022).

The internal velocity dispersions of low-mass ETGs remain systematically too high also in MOND, when compared to their visible stellar mass, while not as much as in the Λ CDM-model (Tortora et al. 2014; Dabringhausen et al. 2016). This could be a consequence of out-of-equilibrium dynamics in Newtonian dynamics (Kroupa 1997; Casas et al. 2012), as well as in Milgromian dynamics (McGaugh & Wolf 2010).

A missing mass problem is also extensively documented for the ETGs at the bright end of the galaxy luminosity function, even though the mass discrepancy detected for them is not as spectacular as the one in spiral galaxies or low luminosity ETGs. However, the question is whether the ETGs all have a universal stellar initial mass function (IMF) and a non-baryonic dark matter component comparable to the mass in stars, or whether the IMF itself changes from ETG to ETG.

The reference model for a non-changing, canonical IMF is given as

$$\xi(m) = k k_i m^{-\alpha_i}, \quad (1)$$

with

$$\alpha_1 = 1.3 \text{ if } 0.1 \leq \frac{m}{M_\odot} < 0.5,$$

$$\alpha_2 = 2.3 \text{ if } 0.5 \leq \frac{m}{M_\odot} < 1.0,$$

$$\alpha_3 = 2.3 \text{ if } 1.0 \leq \frac{m}{M_\odot} \leq m_{\max}$$

(Kroupa 2001; Kroupa et al. 2013), or a function that cannot be distinguished from it with observations (e.g. Chabrier 2003; Dabringhausen et al. 2008). In the above function, m is the initial stellar mass, m_{\max} is the maximum initial stellar mass, the factors k_i ensure that the IMF is continuous where the power changes and k is a normalization constant. The parameter k ensures that the integral over the IMF equals unity, even if the other parameters change. There is some debate over the correct value for m_{\max} in equation 1, as is evident by the differences in m_{\max} in the papers by, for example, Bruzual & Charlot (2003) ($m_{\max} = 100 M_\odot$), Weidner & Kroupa (2004) ($m_{\max} \approx 150 M_\odot$) and Crowther et al. (2010) ($m_{\max} \approx 300 M_\odot$). This has however almost no consequences for mass estimates from equation 1, since for this value of α_3 , the total number of stars with masses $m > 100 M_\odot$ is extremely small compared to stars with lower masses.

The reason why such a stellar population is so popular as a reference is that, for a long time, it appeared that equation 1 is consistent with observations of all stellar populations in the Milky Way (Kroupa 2001; Kroupa et al. 2013). It is thus remarkable that the virial masses of high-luminosity ETGs can in general not be explained with it. This is shown e.g. in Cappellari et al. (2006); Bolton et al. (2008); Tortora et al. (2009); Cappellari et al. (2012); Samurović (2014) and Dabringhausen et al. (2016), even though these authors discuss different solutions to the problem (i.e. changing IMFs, CDM or MOND, and sometimes more than one of these).

If no non-baryonic dark matter is to be invoked, the solution may be an IMF that changes from galaxy to galaxy, which leads to the theory of the integrated galaxy-wide stellar initial mass functions (IGIMFs). The IGIMF-theory is based on the conjecture that all stars form in groups or embedded star clusters, and never in isolation (Kroupa 1995). All the stars that form in the different star clusters of a galaxy over a certain time make up its IGIMF (Kroupa & Weidner 2003), and the mass of the most massive star in a specific star cluster depends on the mass of the star cluster (Weidner et al. 2010; Yan et al. 2017). The mass of the most massive star cluster in a galaxy depends

in turn on the star formation rate (SFR) of the galaxy (Weidner et al. 2004), and already from this, it is evident that no universal galaxy-wide IMF, or IGIMF can exist among galaxies. However, Dabringhausen et al. (2008, 2009, 2012) and Marks et al. (2012) found that also the high-mass slope of the IMF in star clusters, i.e. α_3 in equation 1, depends on their mass, so that it is shallower in more massive star clusters. Thus, very massive star clusters contain more massive stars not only in total, but also per unit of low-mass stars. Moreover, Marks et al. (2012) found an increase of low-mass stars with the metallicity of the star clusters. After some more studies on the variations of stellar populations among galaxies due to the IGIMF-theory (Weidner et al. 2011, 2013a,b; Fontanot et al. 2017; Yan et al. 2017), this was put together by Jeřábková et al. (2018) into a grid of modelled stellar populations, whose high-mass IMF slopes and most massive stars depends on their SFR, and whose low-mass IMF depends on their metallicity. These changes in the stellar populations can explain the overabundance of low-mass stars in massive, and thus metal-rich ETGs (e.g. van Dokkum & Conroy 2010; Cappellari et al. 2012; La Barbera et al. 2013, 2019; Smith 2020; Gu et al. 2022). Other studies on the same topic revealed that there is a gradient in the IMF of the massive ETGs in such a way, that it was extremely over-abundant in low-mass stars especially at their centres, while in their outer parts it approaches the canonical IMF (e.g. La Barbera et al. 2016; van Dokkum et al. 2017; Parikh et al. 2018; Sarzi et al. 2018; Bernardi et al. 2018; Domínguez Sánchez et al. 2019; La Barbera et al. 2019). In the context of the IGIMF-theory, this could mean that present-day star formation with high metallicities happens mainly at the centre of the ETGs, whereas earlier on the star forming regions were more extended. Also a lack of high-mass stars was detected in low-mass late-type galaxies (Lee et al. 2009). The IGIMF-theory can also explain an overabundance of massive stars in the most massive star clusters (UCDs, Dabringhausen et al. 2008, 2009, 2012; Marks et al. 2012). Finally, it can explain the colour dependency of star-forming disk galaxies (Lee et al. 2009; Gunawardhana et al. 2011), or their element abundances and their ratios (Romano et al. 2017; Zhang et al. 2018; Yan et al. 2020, 2021). With a universal IMF for all galaxies, all of this would be difficult, if not impossible.

In other words, we propose the IGIMF-model as the common model for how stellar populations emerge from star formation, in dependence of the size, star-formation rate and metallicity of a given star-forming gas-cloud. This has notably consequences for the massive ETGs, for which many of the above authors claim that their IMFs in their centres are exclusively bottom-heavy. According to the IGIMF-model, this is only true for their most recent star-formation events, which have moderate SFRs and are already enriched with metals. In their past however, when they were less enriched with metals and their star formation rates were high, their IGIMFs were top-heavy according to the IGIMF-model. Massive stars burn out fast, and contribute then only the mass of their remnants to the total masses of their ETGs. Thus, in total, massive ETGs are heavier than what can be explained with a purely canonical IMF because of a combination of bottom-heavy star formation today and top-heavy star-formation in the past. This could in prin-

ciple be checked by testing whether the line indices of the low-mass stars propose enough low-mass stars to account for the missing mass in total (Kroupa & Gilmore 1994). That additional missing mass might be needed, despite the proposed bottom-heaviness of the IMF, was already hinted at in van Dokkum & Conroy (2010).

In this contribution, we will deal with the mass estimates for ETGs with and without the IGIMF-theory. Most of the massive ETGs have formed their stellar populations Gyrs ago, which implies that massive stars have already evolved into remnants in them. In consequence, these stars no longer contribute significantly to the optical luminosity of the ETGs, while the remnants still contribute to their mass. Efforts to link the star formation histories of ETGs with their present-day masses have shown that the characteristic timescale for building up their stellar populations decreases with increasing mass (Thomas et al. 2005; Recchi et al. 2009; Yan et al. 2021). Thus, the most massive (and most luminous) ETGs also had the highest SFRs in the past. Therefore the most luminous ETGs should, according to the IGIMF model, have the most stellar remnants per unit mass of low-mass stars. This could in principle explain the mass deficit detected for them, if their IGIMF is wrongly assumed to be identical to the IMF given in equation (1). We will however not deal with the metallicity dependence of the IGIMF, as the luminosity of the ETGs is an observable. It came to be in its present magnitude whatever the history of a galaxy was, including changes of its IGIMF with metallicity. In this sense, the luminosity is similar to the internal velocity dispersions and the half-light radii, which are the observational basis for the dynamical masses of the galaxies, i.e. the other key observational parameter of the galaxies in this paper.

Thus, the question is probed whether the mass-discrepancy evident in ETGs disappears, if the independently formulated IGIMF model is adopted to quantify the stellar populations in ETGs. Newtonian gravitation and MOND with either the standard μ -function (Milgrom 1983a) or the simple μ -function (Famaey & Binney 2005) are tested in this paper. For this, the concept of radial acceleration relations (RAR) is used, which are discussed by e.g. Wu & Kroupa (2015); McGaugh et al. (2016) or Lelli et al. (2017). RARs emerge essentially by the comparison between the acceleration implied by the observed dynamics of galaxies with the acceleration expected based on the matter density profile of the same galaxies. The latter is at least to some extent based on models and assumptions (such as virial equilibrium, the mass-to-light ratio of the stellar population, the presence of an CDM-halo, etc), and the RAR thereby becomes a powerful tool to test such models and assumptions.

This paper is organized as follows. Section (2) describes the specific data on ETGs from Dabringhausen & Fellhauer (2016) that are used for linking IGIMF-related parameters of ETGs to their observed properties. Section (3) introduces the IGIMF-model, including some adjustments and parameterisations of the IGIMF introduced in Dabringhausen (2019), and used in this paper. In Section (4) our results are laid out, and a discussion is given in Section (5). This is followed by a summary and conclusion in Section (6).

2 DATA

2.1 Selection criteria for the sample of ETGs

The data that are used to link the IGIMF to observed early-type galaxies are provided in the catalogue by Dabringhausen & Fellhauer (2016). This catalogue comprises 1715 ETGs, which span the whole luminosity range of ETGs from faint dwarf spheroidal galaxies (mostly from the catalogue by McConnachie 2012) to giant elliptical galaxies (to a large extent from the ATLAS^{3D} survey, Cappellari et al. 2011). What motivates to combine these galaxies into a single catalogue, and similar galaxies from other sources as well, is that they share two properties: There is little, if any, star formation in them at present, and random motion dominates over ordered motion for their stellar populations. Apart from these two defining properties, the properties of the ETGs are diverse. However, ETGs gather close to a (one-dimensional) line in the (two-dimensional) mass-radius space. This is similar to main-sequence stars (see e.g. Demircan & Kahraman 1991 for the stars).

The quantities from that catalogue that are relevant for the present paper are the effective half-light radii of the ETGs, R_e , their Sérsic indices, n , their observed central line-of-sight (LOS) velocity dispersions, σ_0 , the rotational velocities within their effective radii, v_{rot} , the masses of their stellar plus remnant populations under the assumption that the IMF is canonical, M_{can} , the luminosity in the V -band, L_V . Also a time, t , that represents the overall age of the stellar population and a metallicity, Z , that gives the average metal content of the stars are collected from Dabringhausen & Fellhauer (2016). These ages and metallicities are provided by the literature that Dabringhausen & Fellhauer (2016) used, and are thus subject to the assumptions made there. The parameters R_e , n and σ_0 are needed for estimating the dynamical mass of the galaxies, which are in turn needed for estimating a characteristic radial acceleration that particles seem to experience based on their dynamics, a_{dyn} . M_{can} is not only needed for comparing it to M_{dyn} , but also for estimating their SFR at the time when the majority of their stars formed, SFR_{peak} . L_V plays a crucial role in the estimate of M_{can} . The availability of these data restrict the catalogue from 1715 ETGs to 462 ETGs, which however still cover the almost whole luminosity range of ETGs, from $L_V \approx 10^4 L_{\odot}$ to $L_V \approx 10^{11} L_{\odot}$.

The data on v_{rot} are also collected, since rotation may provide a notable contribution to the overall kinetic energy of the matter in the ETGs. Thus, it is relevant for mass estimates based on the virial theorem. If also v_{rot} is considered, the number of galaxies discussed is limited from 462 to 310. However, the availability of v_{rot} is not made a requirement for a galaxy to be discussed in this paper. We rather examine the full sample at the expense of ignoring v_{rot} , and a subsample, where v_{rot} is considered. This is also done because the galaxies, for which v_{rot} was not measured, lie mostly at low luminosities and masses. Note that v_{rot} in the subsample may still be consistent with zero; the important point is that they were measured.

We refer the reader to Dabringhausen & Fellhauer (2016) for a detailed description of the full catalogue. Additional Information on the restrictions made on this catalogue, so that only 462 galaxies remain for the present paper,

are given in Dabringhausen et al. (2016) and Dabringhausen (2019). While the subset of 462 galaxies used in this paper is exactly the same as in Dabringhausen (2019), some specifics are especially relevant here. They will be detailed in this Section.

2.2 Luminosities

Dabringhausen & Fellhauer (2016) collected luminosities in many passbands, and Dabringhausen (2019) compared these data from different passbands to each other. Here on the other hand, we restrict ourselves to the data on the L_V passband. The reason is that the sample on L_V is the largest data sample among the luminosities in Dabringhausen & Fellhauer (2016), from direct measurements of individual galaxies as well as from derivations from statistical data. Choosing e.g. the I passband instead would narrow the remaining ETGs from 462 to 347.

2.3 Stellar masses and metallicities of the stellar populations

The estimates on M_{can} given in Dabringhausen & Fellhauer (2016) are based on a large set of models for simple stellar populations (SSPs) by Bruzual & Charlot (2003). These SSPs are defined as stellar populations that have formed instantly at a certain time with a certain metallicity.

Dabringhausen & Fellhauer (2016) obtained M_{can} of a given ETG by first searching an SSP-model by Bruzual & Charlot (2003) that represents the age and the colour of the ETG the best. For the ETGs considered in this paper, estimates for age and metallicity were already given in the source papers of Dabringhausen & Fellhauer (2016). Thus, they simply adopted the M_{can}/L_V predicted by the according SSP-model as the M_{can}/L_V of the ETG. Finally, they multiply this M_{can}/L_V by the L_V of the ETG.

There are certainly more elaborate methods to determine the stellar mass M_{can} of a ETG. For instance, the less massive the ETG is, the longer star formation tends to last in it (e.g. Thomas et al. 2005 and Weisz et al. 2014). Thus, instant star formation is becoming an ever rougher sketch to their true star formation history the less massive the ETG is. In such cases, the adopted ages and metallicities can imagined best as characteristic values. On the other hand, this paper does resolve the age-metallicity degeneracy (Worthey 1994) to some extent, as it leaves the ETGs some freedom regarding their best-fitting ages and metallicities. This stands in contrast to some other rather recent papers, which keep the age fixed (e.g. Forbes et al. 2008; Forbes & Kroupa 2011; Misgeld & Hilker 2011), or are even equivalent to keeping age and metallicity fixed (e.g. McConnachie 2012 by assuming a mass-to-light ratio of one in Solar units for every galaxy in his sample).

Recall however the main purpose of this Paper. It is *not* to estimate the masses of individual galaxies as precisely as possible. For this, the method of fits by multiple SSPs by e.g. Blanton & Roweis (2007) or Cappellari et al. (2013b) would evidently be better than the fit to only a single SSP done here, but also far more complicated. Instead, our goal is to show that with MOND and the IGIMF, it is much better possible to understand the dynamics of the *ensemble*

of ETGs without non-baryonic dark matter, in contrast to without these concepts.

2.4 Effective half-light radii

The projected half-light radii, R_e , published in Dabringhausen & Fellhauer (2016) are based on observed values from a multitude of papers. If angular radii are published in their sources, Dabringhausen & Fellhauer (2016) transform them into pc using the distance estimates they adopted for the galaxies in their catalogue. Values for R_e given in parsec in the source papers are transformed by Dabringhausen & Fellhauer (2016) into angular radii using the distance estimates given in the source papers, and then transformed back into parsec again using the respective distance estimates listed in Dabringhausen & Fellhauer (2016).

Most R_e for the massive galaxies come initially from the ATLAS^{3D}-study (Cappellari et al. 2011). More specifically, Dabringhausen & Fellhauer (2016) took the R_e from Cappellari et al. (2013a), which is the same source they used for the velocity dispersions of the respective ETGs. However, Cappellari et al. (2013a) only took the luminosities they could observe within their fields of view, and calculated their R_e on this basis. As a matter of principle, these values for R_e are somewhat smaller than values for R_e , which are calculated from the luminosities of the ETGs with infinite radii.

Finding out the correct R_e for massive ETGs is a tricky business. When Cappellari et al. (2013a) compared their values for R_e with the values they have obtained for the R_e of the same ETGs in Cappellari et al. (2011), they find that they have to multiply the new values by a factor of 1.35 in order to match the old values. However, the fit is excellent then. The reason is probably that the R_e in Cappellari et al. (2011) are normalised such that they correspond on average to the reference catalogue by de Vaucouleurs et al. (1991), who extend the radii of their galaxies to infinity. Cappellari et al. (2013a) on the other hand want to avoid the assumptions involved in extending the luminosity profile to infinity, and cut the ETGs to the field of view of the telescope they used. We nevertheless multiply the R_e from Cappellari et al. (2013a) with 1.35, in concordance to what they did for their analysis as well.

Other contributions to the R_e -values of massive ETGs in Dabringhausen & Fellhauer (2016) come from Bender et al. (1992) and Scodreggio et al. (1998), even though minor compared to the contribution by Cappellari et al. (2013a). In fact, the contribution by Bender et al. (1992) disappears, if also information on rotations is required (see Section 2.7). However, in contrast to the data on R_e from Cappellari et al. (2013a), the R_e from these sources are left unchanged, because the luminosity profiles were already extrapolated to infinity in the source papers.

Also for the remaining ETGs, which are almost exclusively dwarf galaxies, we take the values for R_e unchanged, for reasons explained in Section 2.5.

2.5 Sérsic indices

The Sersic index (Sersic 1968) is the number n that best describes the overall luminosity profile of the galaxy in a generalised luminosity profile of the form

$$I(R) = \frac{L}{R_e^2} \frac{b^{2n}}{2\pi n \Gamma(2n)} \exp \left[-b_n \left(\frac{R}{R_e} \right)^{\frac{1}{n}} \right], \quad (2)$$

where $I(R)$ is the surface brightness of the galaxy as a function of the projected radius R , I_0 is the central surface brightness, R_e is the effective radius and Γ is the gamma-function (e.g. Sérsic 1963; Bernardi et al. 2018). The parameter b_n can be approximated as $b_n \approx 2n - 0.324$ (Ciotti 1991).

In the catalogue by Dabringhausen & Fellhauer (2016), n is adopted from the literature they used, if available there. If not, they calculate n from R_e , using

$$\log_{10}(n) = 0.28 + 0.52 \log_{10} \left(\frac{R_e}{\text{kpc}} \right), \quad (3)$$

which is a relation that Caon et al. (1993) derived from observational data.

Thus, n grows with the R_e of an ETG, which in turn tends to get larger with its mass. So especially for the massive ETGs with their larger R_e and n , the density profiles of the ETGs stretch more to the outer regions. This is even the case if R_e would remain the same with growing n , as is apparent from figure 1 in Ciotti (1991). Because of this behaviour of n , it is particularly the large ETGs with $n \gtrsim 4$ that must be covered fully by their observations, or else their R_e would appear smaller than they actually are. Cappellari et al. (2013a) have indeed found a correction factor by which they have to multiply their massive ETGs, which they have observed only to finite radii. Otherwise they would not match on average the values suggested for the same galaxies with unlimited radii (de Vaucouleurs et al. 1991; Cappellari et al. 2011, Section 2.4 in this paper).

For the other ETGs, their luminosity profiles have either been extrapolated to infinity in their sources, or they are dwarf galaxies. Dwarf ETGs mostly have $1 \lesssim n \lesssim 2$, and are thus more centrally concentrated than the massive ETGs (see figure 1 in Ciotti 1991). Therefore, cutting off the outer parts of the dwarf galaxies is much less problematic than with the massive ETGs, and for this reason, also their R_e are adopted unchanged from the catalogue by Dabringhausen & Fellhauer (2016).

2.6 Velocity dispersions

In the context of the present paper, we have to distinguish carefully between the expected line-of-sight (LOS) velocity dispersion of the tracer population due to the gravitational potential of the ETG, and the observed LOS velocity dispersion. We denote the former as σ_0 , and the latter as σ_{obs} . σ_0 is completely unordered motion, while σ_{obs} is not always. Also the two quantities are often used interchangeably, while they not always are.

As an example for $\sigma_0 \neq \sigma_{\text{obs}}$, consider a tracer population of binary stars. In this case, $\sigma_{\text{obs}} > \sigma_0$, because the stars in the binary move around their common centre of mass, while the binary systems as wholes move due to the

potential of the galaxy. The former is completely unrelated to the potential of the galaxy, but nevertheless adds to σ_{obs} .

Now consider a rotating galaxy, or more generally, a galaxy where the mean velocity towards the observer changes over the field of view. Also this case implies $\sigma_{\text{obs}} > \sigma_0$, because σ_0 only quantifies the unordered motion, while σ_{obs} stems from both the ordered and the unordered motion within the field of view. The effect from ordered motion can in theory be eliminated by decreasing the field of view until only the centre of the ETG is observed, but this is in practice only possible up to a certain point. However, in contrast to binaries, rotation has the same cause as the unordered motion, namely the overall gravitational field of the galaxy. Therefore it cannot be separated easily from σ_0 .

Dabringhausen & Fellhauer (2016) follow the usual convention by designating the central LOS velocity dispersions of the ETGs as σ_0 , while the quantities that they actually list in their catalogue are values for σ_{obs} according to the above definitions for σ_0 and σ_{obs} . Their data on σ_{obs} are taken from the literature they use, if such a value was published there. If only the *average* observed LOS velocity dispersion within R_e , σ_e , is available from the literature they use, they estimate σ_{obs} using the relation

$$\log_{10} \left(\frac{\sigma_{\text{obs}}}{\text{km/s}} \right) = 1.0478 \log_{10} \left(\frac{\sigma_e}{\text{km/s}} \right) - 0.0909, \quad (4)$$

which is obtained from a least-squares fit to data on 260 ETGs in Cappellari et al. (2013a), see the upper panel of their figure 8. Dabringhausen & Fellhauer (2016) thus take the data on the velocity dispersions within the central parsec of the ETGs in Cappellari et al. (2013a) as a measure for σ_{obs} . Equation (4) can therefore not be used on ETGs with $R_e < 1$ kpc by construction, which is why Dabringhausen & Fellhauer (2016) set $\sigma_{\text{obs}} = \sigma_e$ for such ETGs. This is well motivated by the findings that $R_e = 1$ kpc corresponds to $n \approx 1.9$ according to equation (3), and that the velocity dispersion profiles of galaxies with $n \lesssim 2$ are almost flat within their R_e (see Graham & Colless 1997, their figure 8).

How relevant rotation (i.e. ordered motion) and binaries actually are for mass estimates of ETGs will be discussed in more detail in Sections (3.6) and (3.7).

2.7 Rotational velocities

Dabringhausen & Fellhauer (2016) aim at giving the rotational velocity of the ETGs, v_{rot} , as the average rotational velocity of the ETG within R_e , but the provided data in the source literature is quite heterogeneous. Actual estimates for the average rotational velocity are mainly given for luminous ETGs, whose extension and surface brightness allow to take independent spectra from many patches within R_e , and derive the underlying motions for each of these spectra. Less luminous galaxies are at a given distance more challenging to observe in detail than their more luminous counterparts. Estimates of their rotation therefore tend to be based on fewer individual telescope pointings, and are usually rather quantified through maximum rotational velocities or the rotational velocities at R_e instead of proper averages within R_e .

The data for v_{rot} provided by Dabringhausen & Fellhauer (2016) may however be more

comparable than it may seem from the inhomogeneities in the data in the source papers. By construction, the average rotational velocity is smaller than the maximum rotational velocity, which however is reached well within R_e for many low-luminosity ETGs (Geha et al. (2003)). Therefore, the average rotational velocity may for these ETGs actually be quite close to the maximum rotational velocity. On the other hand, there are also low-luminosity ETGs for which the rotational speed may still increase outside R_e . Thus, an estimate for the rotational velocity for such ETGs at the radius R_e is smaller than the maximum rotational velocity, but is again probably quite close to it.

3 METHODS

3.1 The IGIMF...

The fundamental assertions for the IGIMF is that most, if not all stars form in groups and not in isolation (Kroupa 1995), and that the IMFs in these groups are not universal, but depend on star formation conditions.

The metallicity determines the abundance of low-mass stars in IMFs in such a way that their number increases with metallicity. Kroupa (2002) and Marks et al. (2012) use the equation

$$\alpha_i = \alpha_{ic} + \Delta\alpha \times [\text{Fe}/\text{H}] \quad (5)$$

for $i = 1$ and $i = 2$ in equation 1 for this, i.e. for stellar masses $m \leq 1M_{\odot}$. α_{ic} are the low-mass IMF slopes of the canonical IMF (equation 1). For α_3 in equation 1, i.e. for $m > 1M_{\odot}$, Marks et al. (2012) find

$$\alpha_3 = \begin{cases} 2.3 & \text{if } x < -0.87 \\ 1.94 - 0.41x & \text{if } x \geq -0.87, \end{cases} \quad (6)$$

with

$$x = -0.14 \times [\text{Fe}/\text{H}] + 0.99 \times \log_{10} \left(\frac{\rho_{\text{cl}}}{10^6 M_{\odot} \text{pc}^{-3}} \right). \quad (7)$$

In the above equation, ρ_{cl} is the density of the embedded star cluster, i.e. of the star-forming molecular cloud core, or in other words, the infant star cluster still containing the left-over gas besides the stars. Thus, the number of massive stars mostly increases with ρ_{cl} , corrected by a small decrease with rising metallicity. The equation

$$\frac{r_{\text{h}}}{\text{pc}} = 0.10 \times \left(\frac{M_{\text{ecl}}}{M_{\odot}} \right)^{0.13}, \quad (8)$$

connects ρ_{cl} with the mass of the embedded cluster, M_{ecl} , over its average 3D half-light radius, r_{h} . The mass of the most massive star cluster that can form in a galaxy, $M_{\text{ecl,max}}$, depends on the SFR of the galaxy as

$$\frac{M_{\text{ecl,max}}}{M_{\odot}} = 84793 \times \left(\frac{\text{SFR}}{M_{\odot} \text{yr}^{-1}} \right)^{0.75}, \quad (9)$$

according to Weidner et al. (2004). The star cluster mass determines in turn the mass of its most massive star (Weidner et al. 2010; Yan et al. 2017). A parametrisation of the dependence of the mass of the most massive star, m_{max} ,

on M_{ecl} is

$$\begin{aligned} \log_{10}(m_{\text{max}}) &= 2.56 \log_{10}(M_{\text{ecl}}) \\ &\times (3.82^{9.17} + [\log_{10}(M_{\text{ecl}})]^{9.17})^{(1/9.17)} - 0.38, \end{aligned} \quad (10)$$

(Pflamm-Altenburg et al. 2007). All star clusters and stellar groups of a galaxy with their different IMFs produce over a certain time its IGIMF, as introduced by Kroupa & Weidner (2003). The shortest time span that is thought to populate the IGIMF of a galaxy completely is about 10 Myr (Weidner et al. 2004), the average lifetime of molecular clouds.

3.2 ...and its simplification

Jeřábková et al. (2018) collected this information into a grid of IMFs that depend on the metallicities in which the stars form and on the SFR, and plotted a sample of these in their figure 1. Generally, the metallicity and the star formation in ETGs are low at first, then both rise, and finally the SFR is low again while the metallicity is high. This is shown in fig. 2 in Jeřábková et al. (2018), which illustrates that indeed a few star clusters form with IMFs like in the snapshots in figure 1 with extreme metallicities early in the life of the galaxy, but many more with IMFs more akin the canonical IMF later on.

More importantly is however that the quantities that are looked at in this paper are rather insensitive to the exact shape of the resulting IGIMF. This is notably also the case at its lower end, where the IGIMF is especially sensitive to the metallicity. We are however not interested in colours (like e.g. Gunawardhana et al. 2011) or ratios of line indices (like e.g. van Dokkum & Conroy 2010) in order to measure the shape of the low-mass IGIMF. Instead, the L_V -luminosities are the only quantity connected to the light of the galaxies that we care about, independently of the slope or shape of low-mass IGIMF that produces it. It is therefore safe in the context of this paper to set the IGIMF to constant values below masses of $1 M_{\odot}$ for a simplification.

Above masses of $1 M_{\odot}$, there is a weak dependency on metallicity as well, but we neglect it over the much stronger dependency on the SFR in this mass range. Thus, as in Fontanot et al. (2017), we consider for this paper the IGIMF on its whole mass-range only as a function of SFR of a galaxy, and not on its metallicity.

Dabringhausen (2019) simplified the IGIMFs of the ETGs even further to

$$\xi_{\text{IGIMF}}(m) = k k_i m^{-\alpha_i}, \quad (11)$$

with

$$\begin{aligned} \alpha_1 &= 1.3 \text{ if } 0.1 \leq \frac{m}{M_{\odot}} < 0.5, \\ \alpha_2 &= 2.3 \text{ if } 0.5 \leq \frac{m}{M_{\odot}} < 1.0, \\ \alpha_{\text{eff}} &\in \mathbb{R} \text{ if } 1.0 \leq \frac{m}{M_{\odot}} \leq m_{\text{max}}, \end{aligned}$$

where m is the initial stellar mass, m_{max} and α_{eff} are SFR-dependent parameters, the factors k_i ensure that the IGIMF is continuous where the power changes and k is a normalization constant that ensures that the integral over the IGIMF equals unity, even if the other parameters change. Although

this IGIMF looks from its parametrisation very similar to the IMF given in equation 1, it is based on a completely different concept.

The values by Fontanot et al. (2017) for the SFR-dependent mass of the most massive stars, m_{max} , is parametrized by Dabringhausen (2019) as

$$\begin{aligned} \frac{m_{\text{max}}}{M_{\odot}} &= \left[\log_{10} \left(\frac{SFR}{M_{\odot} \text{yr}^{-1}} \right) + 5.824 \right]^{3.133} \\ &- 0.4086 \times \log_{10} \left(\frac{SFR}{M_{\odot} \text{yr}^{-1}} \right) \end{aligned} \quad (12)$$

for $\log_{10}(SFR/M_{\odot} \text{yr}^{-1}) < -0.878$, and $m_{\text{max}} = 150 M_{\odot}$ for $SFR \geq -0.878 M_{\odot} \text{yr}^{-1}$. Thus, the physical mass limit for stars is set here to $150 M_{\odot}$, in concordance with Weidner & Kroupa (2004) and Oey & Clarke (2005). Even more massive stars may form (Crowther et al. 2010) from the mergers of binaries (Banerjee et al. 2012a,b). Their frequency is strongly suppressed, though, as also their progenitor stars are rare by the power α_3 in equation (1). Thus, a higher value for m_{max} has little effect on the results presented in this paper.

Finally, the SFR-dependent value of α_{eff} is given as

$$\alpha_{\text{eff}} = -1.2250 \log_{10} \left(\frac{SFR}{M_{\odot} \text{yr}^{-1}} \right) - 1.4558 \quad (13)$$

if $\log_{10}(SFR/M_{\odot} \text{yr}^{-1}) \leq -3.9110$,

$$\alpha_{\text{eff}} = -0.23859 \log_{10} \left(\frac{SFR}{M_{\odot} \text{yr}^{-1}} \right) + 2.4021 \quad (14)$$

if $-3.9110 < \log_{10}(SFR/M_{\odot} \text{yr}^{-1}) \leq 3.3900$, and

$$\alpha_{\text{eff}} = -0.05060 \log_{10} \left(\frac{SFR}{M_{\odot} \text{yr}^{-1}} \right) + 1.7648 \quad (15)$$

if $\log_{10}(SFR/M_{\odot} \text{yr}^{-1}) > 3.3900$. We do follow this parametrization, but in practice, the effective high-mass slopes of almost all ETGs in the sample discussed here are given by equation 14 (see also section 3.2 in Dabringhausen 2019).

3.3 Linking the IGIMF to observed parameters of early-type galaxies

While the SFR correlates with the shape of the IGIMF in galaxies, it is not the most practical parameter for estimating a characteristic IGIMF in early-type galaxies (ETGs) from directly observable quantities. The reason is that the present-day SFR in ETGs is so low that the present-day masses of their stellar populations imply that the SFR must have been much higher when the majority of their stars have formed. However, the abundance of α -elements can serve as an indirect indicator for the SFR of an ETG in the past. The underlying notion is that different types of supernovae reinserted different mixtures of elements into the interstellar medium (ISM) on different timescales, from which new stars were still forming. Type-II supernovae, which have high yields of α -elements, are thought to be the final stage of the evolution of high-mass stars and therefore occur on a timescale of Myr after the formation of their progenitor stars. Type-Ia supernovae on the other hand, which have high yields of iron, are thought to be white dwarfs that

surpass the Chandrasekhar-mass by accreting matter. Depending on the parameters of the progenitor binary system, it can take individual binaries Gyrs until one of the components becomes a SNIa, while the peak in the SNIa rate in a typical ETG is at a timescale of approximately 0.3 Gyr according to Matteucci & Recchi (2001). The key point is that the delay for SNIas in a galaxy is in any case longer than the delay for SNIIs. This is because SNIIs are linked to the timescale for the evolution of massive stars while SNIas require the remnant of an intermediate or low mass star. As a consequence, the SNIIs associated to a given star formation event naturally precede the SNIas associated to the same event. Long-lasting star formation leads however to a continuing production of both SNII and SNIa progenitors, and after a while newly forming stars can use preprocessed material from SNIa and SNII alike. This suggests that the higher the α -abundance in a stellar population of a ETG is in comparison to its iron-abundance, the sooner the ETG must have stopped to form stars.

On this basis, Yan et al. (2021) have estimated the timescales for the formation of ETGs of different mass. They find

$$\frac{\tau}{\text{Gyr}} = \begin{cases} 0.003 \left(\frac{M_{\text{IGIMF}}}{M_{\odot}} \right)^{0.3} & \text{for } \frac{M_{\text{IGIMF}}}{M_{\odot}} \leq 5 \cdot 10^9 \\ 49 \left(\frac{M_{\text{IGIMF}}}{M_{\odot}} \right)^{-0.14} & \text{for } \frac{M_{\text{IGIMF}}}{M_{\odot}} > 5 \cdot 10^9 \end{cases} \quad (16)$$

where τ is an estimate for the total time that it takes the galaxy form most of its stars and M_{IGIMF} is an estimate for the stellar mass of an ETG according to the IGIMF-model. Note that stellar remnants are included in M_{IGIMF} . How M_{IGIMF} is calculated in this paper, including M_{can} as a special case for when the IMF is canonical, is described in Section 3.4.

For ETGs with $M_{\text{IGIMF}}/M_{\odot} \leq 5 \cdot 10^9$, equation 16 is a fit to the most probable values for the star formation times according to GALIMF¹, a program which combines the IGIMF theory with a model for the chemical evolution of galaxies (Yan et al. 2019a).

In contrast to ETGs with $M_{\text{IGIMF}}/M_{\odot} \leq 5 \cdot 10^9$, several attempts have been made for ETGs with $M_{\text{IGIMF}}/M_{\odot} > 5 \cdot 10^9$ to relate their star formation times to their mass (e.g. Thomas et al. 2005; de La Rosa et al. 2011; McDermid et al. 2015). The best fit to the results from GALIMF proves to be the relation from McDermid et al. (2015), if their equation 3 is combined with equation 3 in Thomas et al. (2005) to translate $[\alpha/\text{Fe}]$ into masses. This relation, and not some new fit from GALIMF to data, is taken for equation 16 for galaxy masses $M_{\text{IGIMF}}/M_{\odot} > 5 \cdot 10^9$ (see figure 7 in Yan et al. 2021).

Thus, for high-mass ETGs, the masses are stellar masses (including stellar remnants) and the IMF is canonical, because equation 3 in Thomas et al. (2005) is given in these quantities as well. In other words, the mass entering the calculations of their star formation times is M_{can} . However, it has been argued in Yan et al. (2019b) that M_{can} can be exchanged with M_{IGIMF} without making grave errors, and indeed, replacing M_{can} with M_{IGIMF} in the figures in this paper has only minor effects. However, we carefully distin-

guish between M_{can} and M_{IGIMF} for all other instances in this paper.

The values for the star formation times are nonetheless only indicative anyway. Consider e.g. galaxy mergers, which are known to happen in the Universe (e.g. Toomre 1977). If two galaxies with ongoing star formation collide, the collision is thought to provoke a starburst, which is at least qualitatively consistent with the notion that more massive galaxies form stars more rapidly than lighter galaxies. Now on the other hand, imagine two galaxies that merge after each of them has finished its star formation. According to the picture here, their formation time scales were those of the lighter progenitors, but its mass would be that of the more massive merger remnant. In the end, the time scales for galaxy formation cited here are just statistical numbers that indicate how an average ETG of a certain mass is supposed to evolve, while individual ETGs of that mass can deviate from this value quite strongly.

3.4 The masses of ETGs according to the IGIMF-model

Estimates for the stellar mass of an ETG according to the IGIMF-model, M_{IGIMF} , can be obtained based on existing estimates for M_{can} , i.e. mass estimates that are based on equation (1), and estimates for the masses of evolved SSPs that formed with the IGIMF. The latter are given as

$$M_{\text{pop}}(\alpha_{\text{eff}}) = k_{\text{L}} \int_{0.1}^{m_{\text{max}}} m_{\text{rem}}(m) \xi_{\text{IGIMF}}(m) dm, \quad (17)$$

i.e. by integrating the present-day masses of stars and stellar remnants over the whole range of initial stellar masses. In equation 17, $\xi_{\text{IGIMF}}(m)$ is the IGIMF given by equation 11, M_{pop} is the mass of the stellar population in dependency of α_{eff} in equation 11, m_{max} is the mass of the most massive stars forming in the galaxy and is given by equation (12) for $\log_{10}(SFR/M_{\odot}\text{yr}^{-1}) < -0.878$ or $m_{\text{max}} = 150 M_{\odot}$ for $\log_{10}(SFR/M_{\odot}\text{yr}^{-1}) \geq -0.878$, and $m_{\text{rem}}(m)$ is the initial-to-final mass function, which expresses the masses of stellar remnants as a function of the initial mass. The factor k_{L} is a scaling factor that ensures that the total luminosity of the stellar population below masses of $1 M_{\odot}$ remains constant when α_{eff} varies. This corresponds approximately to the stars that still shine in old populations like the ETGs. This is motivated by the notion that the luminosity is fixed through observations, while the mass of the stellar population is treated here as an unknown parameter that is to be determined. This stands in contrast to k in equation 11, which keeps the integral at unity, independent of the value for α_{eff} . Thus, k has to change with α_{eff} in equation 11.

The initial-to-final mass function used in equation (17) is the one introduced in Dabringhausen et al. (2009), which is designed for stellar systems older than 10^8 years. It is given as

$$\frac{m_{\text{rem}}}{M_{\odot}} = \begin{cases} \frac{m}{M_{\odot}} & \text{if } \frac{m}{M_{\odot}} < \frac{m_{\text{to}}}{M_{\odot}} \\ 0.109 \frac{m}{M_{\odot}} + 0.394 & \text{if } \frac{m_{\text{to}}}{M_{\odot}} \leq \frac{m}{M_{\odot}} < 8 \\ 1.35 & \text{if } 8 \leq \frac{m}{M_{\odot}} < 25 \\ a \frac{m}{M_{\odot}} & \text{if } 25 \leq \frac{m}{M_{\odot}} \leq m_{\text{max}}. \end{cases} \quad (18)$$

m_{max} is given in this equation by equation (12) for $\log_{10}(SFR/M_{\odot}\text{yr}^{-1}) < -0.878$ and else by $150 M_{\odot}$.

¹ <https://github.com/Azeret/galIMF>

Thus, stars with masses below the main-sequence turn-off mass m_{to} are considered to still have their initial masses, white dwarfs are thought to have progenitors with masses between m_{to} and $8 M_{\odot}$ and their masses are given by a relation found by Kalirai et al. (2008) and neutron stars are thought to have progenitors with masses between $8 M_{\odot}$ and $25 M_{\odot}$ and are all considered to have a mass of $1.35 M_{\odot}$, which is observationally supported by Thorsett & Chakrabarty (1999). Stars with initial masses above $25 M_{\odot}$ are considered to evolve into black holes. The mass of these black holes is the most uncertain parameter and strongly depends on their metallicity (compare for example figures 12 and 16 in Woosley et al. 2002). In equation 18, it is simply set to a constant a , $0 \leq a < 1$. Thus, a is a factor anywhere in between the complete destruction of the star, or the almost complete perseveration of the mass of the star in the process of becoming a BH. The case $a = 1$ is impossible, because stars produce winds during their lifetimes. On the other hand, the existence of stellar-mass BHs is well known, either through the detection of X-rays that such a BH emits if it accretes matter (e.g. Clark 1975 and Ivanova et al. 2008), or through the direct detection of gravitational waves in mergers of stellar-mass BHs (Abbott et al. 2016).

We reflect this uncertainty on the mass of the BHs by considering the two cases, which mark the possible extremes to the values that can be obtained.

In the first case, we use the assertion that low BH masses correspond to stars with high metallicities, and high black hole masses to stars with low metallicities. This progression of the mass of the black holes with metallicity is estimated here as

$$a = \frac{m_{\text{BH}}}{m} = -\frac{4}{3}[Z/H] + \frac{1}{6}, \quad (19)$$

where m_{BH} is the mass of the black hole, $[Z/H]$ is the metallicity of the galaxy today and m is the initial mass of the progenitor star. Equation 19 produces black holes that have 0.5 times the mass of the progenitor at $[Z/H] = -2.5$ and decline linearly to 0.1 times the progenitor mass at $[Z/H] = 0.5$. By using the contemporary metallicities of the galaxies, the masses of the BHs are especially for the metal-rich massive ETGs likely to be too low.

In the second case, we maximize the mass of the BHs by setting $a = 1$, i.e. the massive stars have not experienced any mass loss before they evolve to BHs. We do this despite the fact that every star produces a stellar wind, albeit the metal-poor ones much less than the metal-rich ones (e.g. Woosley et al. 2002).

The explicit terms that the integration in equation (17) yields are listed in the appendix to Dabringhausen et al. (2009), provided that 0.1 in their last equation is replaced by $-4/3[Z/H] + 1/6$ for the first case and 1 for the second case.

The estimates for the actual masses of the stellar populations of the ETGs according to the IGIMF-model can then be calculated as

$$M_{\text{IGIMF}} = \left(\frac{M_{\text{pop}}(\alpha_{\text{eff}})}{M_{\text{pop}}(\alpha_{\text{eff}} = 2.3)} \right) \times M_{\text{can}}, \quad (20)$$

where $M_{\text{pop}}(\alpha_{\text{eff}})$ is given by evaluating equation (17) for the α_{eff} implied by the SFR with which the majority of the stellar population of the studied ETG has formed and m_{max} is given by equation (12). $M_{\text{pop}}(\alpha_{\text{eff}} = 2.3)$ is given by eval-

uating equation (17) for $\alpha_{\text{eff}} = 2.3$, and M_{can} is the estimate of the mass that the stellar population of the studied ETG would have with $\alpha_{\text{eff}} = 2.3$. Note that the results of equation 20 can change even for the same value of α_{eff} , if the assumed masses for the stellar-mass BHs change.

As the stellar populations in question are typically much older than one Gyr, all stars that have survived until now have masses around $1 M_{\odot}$, or less. For such stars, the precise ages of the stars do not matter much for the luminosity of their stellar population, if the stellar population follows eq. 11. However, the value of the high-mass slope of the IGIMF, α_{eff} , continues to matter for the mass of the stellar population, and thus also for the mass-to-light ratio. Simply put, the same difference in α_{eff} makes much less of a difference in the relative numbers of stars between $1 M_{\odot}$ and $2 M_{\odot}$ than for stars with masses between, say, $25 M_{\odot}$ and $26 M_{\odot}$. This is explained in detail in section 3.4 in Dabringhausen (2019).

3.5 Dynamical masses

Besides the stellar masses, i.e. mass estimates based on assumptions on the stellar populations of the ETGs, there are also dynamical mass estimates based on the structure and the motions in the galaxies. In its simplest form, some effective radius, a velocity dispersion within this radius, and some density profile are needed for a dynamical mass estimate. More elaborate dynamical mass models could e.g. work with several velocity dispersions from different spots of the same galaxy, or distinguish between velocity dispersions and rotational velocities of a galaxy. The availability of both mass estimates (i.e. dynamical and stellar) is crucial for testing laws of gravity, i.e. the work done here. If both agree with one another within the uncertainties, it means that both ways of measuring the mass of the galaxy yield the same result.

First, we make some assertions, assumptions and definitions on the galaxies in our sample. They are vital for the estimates of their dynamical masses:

- The mass profiles of the galaxies are Sérsic-profiles (Sérsic 1963; see section 2.5), as opposed for example to Plummer-profiles (Plummer 1911) or King-profiles (King 1962). The Sérsic-profiles are more complicated than in particular the Plummer profile, but they are especially adapted to galaxies, and not to star clusters.
- Massive ETGs are known to possess a central peak in their M_{dyn}/L -ratios, indicating more mass per unit luminosity at their centres (van Dokkum & Conroy 2010). Bernardi et al. (2018) model this as

$$\Upsilon = \Upsilon_{\text{can}} [1 + c(\epsilon - \eta(R/R_e))] \quad (21)$$

for R where $\Upsilon > \Upsilon_{\text{can}}$, and $\Upsilon = \Upsilon_{\text{can}}$ otherwise. In this equation, Υ is the mass-to-light ratio at the projected radius R , Υ_{can} is the mass-to-light ratio with the canonical IMF and R_e is the projected half-light radius. The parameter c is given as

$$c = \frac{[\sigma_0/(km s^{-1})] - 100}{250 - 100}, \quad (22)$$

where σ_0 is the central velocity dispersion. For the parameters ϵ and η , Bernardi et al. (2018) give two choices: Either

$\epsilon = 2.33$ and $\eta = 6.0$ based on observation of six massive ETGs by van Dokkum et al. (2017), or a more intermediate case with $\epsilon = 1.29$ and $\eta = 3.33$. Subsequent observation of many more ETGs by Chae et al. (2018) and Domínguez Sánchez et al. (2019) favour the intermediate case. In this paper, this will be done as well, and referred to as the ‘standard case’.

If $\sigma_0 > 100$ km/s and the IGIMF-model is used for estimating the mass of a given ETG, we integrate

$$M = 2\pi \int_0^R I(R) \Upsilon R dR \quad (23)$$

with increments of $dR = 1$ parsec, until $M/M_{\text{IGIMF}} > 0.5$ is reached. $I(R)$ is the Sérsic-profile as given in equation 2, and we start with the Sérsic-index n given in Dabringhausen & Fellhauer (2016). The corresponding value of R is the new half-mass radius, which is smaller than the half-mass calculated with mass following the light of the galaxy. Also n needs to be updated to the new R_e with equation 3. Finding the updated R_e and n is in principle an iterative process, but we stop here after the first iteration.

If the IGIMF-model is not used, or $\sigma_0 < 100$ km/s in the given ETG, then mass follows light.

- Gas and dust are neglected in the ETGs (see Young et al. 2011 for the paucity of gas in ETGs and Dariush et al. 2016 for the paucity of dust).

- The default for the ETGs is an anisotropy parameter, β , at zero (cf. equation 4-53b in Binney & Tremaine 1987). This describes a galaxy that does not rotate and whose systematic patterns in the motions of the stars can be neglected. As a consequence, the dynamical mass of the ETG will be overestimated if $-\infty < \beta < 0$ (i.e. the stellar orbits in the ETG are predominately circular) and underestimated if $0 < \beta < 1$ (i.e. the orbits in the ETG are predominately radial). We also introduce rotation of the galaxies if some value on it was published in Dabringhausen & Fellhauer (2016), and refer the reader to Sections 3.6 to 3.8 in the present paper for details on it.

- The ETGs are in virial equilibrium. This means that the ETG has settled into a configuration where its gravitational potential and thus its density profile does not depend on time. This assumption implies in particular that the ETG are not significantly disturbed by tidal forces, i.e. external, time-dependent gravitational fields. Tidal fields increase the actually observed internal velocity dispersions and may even disrupt galaxies (Kroupa 1997; Fellhauer & Kroupa 2006; McGaugh & Wolf 2010; Casas et al. 2012; Domínguez et al. 2016). Galaxies which are wrongly assumed to be in virial equilibrium when their dynamical mass is estimated, but are in fact subjected to tides, can have dynamical ‘masses’ which are too high by orders of magnitudes.

- The density profiles of the ETGs can be approximated as spherically symmetric. As a consequence of this assumption, we use in the following R_e to estimate the dynamical mass of an ETG (instead of elliptic shapes, for instance). R_e is also used for estimating the characteristic accelerations in the ETGs due to their stellar or dynamical masses.

These assumptions can be cast together into an estimate for the dynamical masses of the galaxies as

$$M_{\text{dyn}} = \frac{K_V}{G} R_e \sigma_0^2, \quad (24)$$

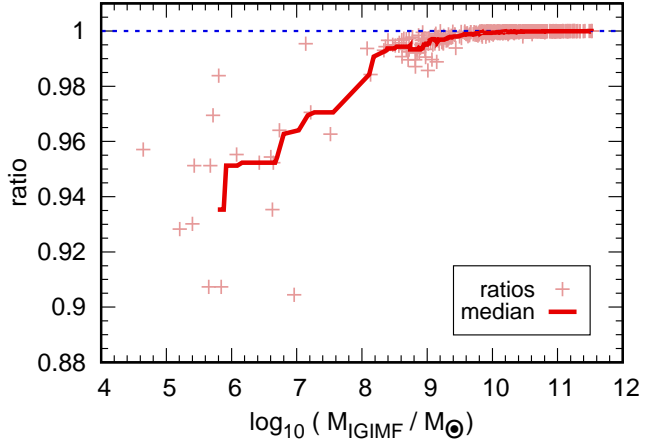


Figure 1. The ratios $M_{\text{dyn}}^{\text{bin}}/M_{\text{dyn}}$ in dependence of M_{IGIMF} for all 462 ETGs in the sample as light red crosses. The thick dark red line indicates for each galaxy the median value of itself and its 20 closest neighbours in M_{IGIMF} . An exception are the ten least massive ETGs and the ten most massive ETGs, for which this quantity cannot be calculated, because this quantity should incorporate 10 ETGs with smaller masses and 10 ETGs with larger masses.

where K_V is a factor that depends on the shape of the density profile of the ETG and G is the gravitational constant. K_V is approximated with equation (11) in Bertin et al. (2002), i.e.

$$K_V(n) = \frac{73.32}{10.465 + (n - 0.94)^2} + 0.954, \quad (25)$$

where n is the Sérsic index. Thus, K_V increases with decreasing n , which in turn decreases with decreasing R_e . If σ_0 is left unchanged, assuming a peak in Υ at the centre of an ETG decreases M_{dyn} compared to Υ being constant throughout the ETG.

The kinetic Energy of an ETG is, under the assumptions in this section,

$$E_{\text{kin}} = \frac{1}{2} M_{\text{dyn}} \sigma_0^2, \quad (26)$$

so that

$$M_{\text{dyn}} = \sqrt{\frac{2 K_V R_e}{G}} E_{\text{kin}} \quad (27)$$

is an alternative way to express equation 24.

The simplest way to estimate a dynamical mass with equation 24 is to take an observed central line-of-sight velocity dispersion, σ_{obs} , and set it equal to σ_0 . However, this approach neglects the effects binaries and the rotation of the galaxies may have on the dynamical mass estimates. Thus, binaries and rotation are introduced in Sections 3.6 to 3.8.

3.6 Binaries

Consider the presence of binaries in the galaxies. The motion of a star in a binary has two components, namely the motion around the centre of mass of the binary and the motion of the centre of mass in the potential of the ETG. The distribution of the line-of-sight motions of the stars in binaries are the consequence of random combinations of many

parameters and processes (such as direction motion in 3D-space, orientation of binaries in 3D-space, excentricities, energy exchange in encounters, and so on). Thus, the central limit theorem implies that this distribution is Gaussian. The motions of stars in binaries and the motions of the stellar systems (i.e. single stars and binary systems) in the ETG are moreover uncorrelated. This means that the observed line-of-sight velocity dispersion of a stellar population is given as

$$\sigma_{\text{obs}}^2 = (1 - f)\sigma_0^2 + f(\sigma_0^2 + \sigma_{\text{bin}}^2), \quad (28)$$

where σ_{obs} is the *observed* central line-of-sight velocity dispersion, σ_0 is the central line-of-sight velocity dispersion of the tracer population due to the *potential* of the ETG and σ_{bin} is the line-of-sight velocity dispersion of stars in *binaries* due to their motions around their common center of mass, f is the fraction of binaries and thus $1 - f$ is the fraction of singles. In principle, also hierarchical higher-order multiples would have to be considered, if present-day stellar populations are dealt with. Their number may seem significant if compared to binaries (see e.g. Raghavan et al. 2010), but in fact every hierarchical multiple system consists of one or more binaries at the bottom of the hierarchy. These binaries are the tightest units of the complete system and their star move thus the fastest around their centres of masses. They would therefore completely dominate the increase of σ_{obs} over σ_0 . Hence, higher order multiples are neglected here, and

$$M_{\text{dyn}}^{\text{bin}} = \frac{K_V}{G} R_e \sigma_0^2 = \frac{K_V}{G} R_e (\sigma_{\text{obs}}^2 - f \sigma_{\text{bin}}^2). \quad (29)$$

is the true dynamical mass of an ETG with binaries under this premise.

According to Marks & Kroupa (2011), the binary fraction f is about 80 percent in very low-mass ETGs, whereas it is about 30 percent in high-mass ETGs. We emulate this dependency by assuming $f = 0.8$ for ETGs with $M_{\text{can}} = 10^3 M_{\odot}$, and then linearly going down with M_{can} , until we reach $f = 0.3$ for ETGs with $M_{\text{can}} = 10^{12} M_{\odot}$. For the value of σ_{bin} , Gieles et al. (2010) derive an analytic approximation, which they formulate as

$$\sigma_{\text{bin}}^2 = \frac{1}{3} \left(\frac{2q^{3/2}}{1+q} \right)^{4/3} \left(\frac{\pi G m_1}{2P} \right)^{2/3}. \quad (30)$$

In this equation, q is the mass ratio of the two components of the binary, m_1 is the typical mass of the more massive component of the binary and P is the typical orbital period in the binaries. In this paper, we use $q = 0.6$ (cf. Gieles et al. 2010), $P = 10$ yr and $m_1 = 1 M_{\odot}$, which leads to $\sigma_{\text{bin}} = 2.3$ km/s in equation (30); see Dabringhausen et al. 2016. Thus, in comparison with the median in P of 180 yr in Duquennoy & Mayor (1991), the binaries are very tight. We therefore maximize their effect on σ_{bin} , and thus on σ_0 , which together have to result in the observable σ_{obs} . Choosing the binaries very tight probably also overcompensates the small error made by ignoring the higher orders of hierarchical stellar systems with more than two stars.

Fig. 1 shows the ratios of the dynamical masses with and without binaries, plotted over the stellar mass of their galaxies according to the IGIMF-model. Especially at low masses, $M_{\text{dyn}}^{\text{bin}}$ is lower than M_{dyn} in selected galaxies, but at high stellar masses, both ways to estimate the mass yield almost

the same results. Note that this is not an effect of the more massive galaxies having fewer binaries (see Marks & Kroupa 2011), but of the more massive galaxies having σ_0 so large that σ_{bin} becomes negligible. This is also the case for our rather generous choice of σ_{bin} .

We calculate also a median of the ratios of $M_{\text{dyn}}^{\text{bin}}$ in dependence of M_{dyn} , which is shown as a solid (red) line in Fig. 1. For obtaining these medians, we consider all ETGs for which the ratios of the mass estimates are known, and number them consecutively by ascending stellar mass. From this list, we construct all possible subsets that contain 21 ETGs with consecutive numbers in stellar mass. These subsets are then sorted with ascending ratios of $M_{\text{dyn}}^{\text{bin}}$ over M_{dyn} , and the 11th highest value among this subset is then chosen as the characteristic value for the ratio of ETGs with the luminosity of the i th ETG. By construction, this method cannot assign a characteristic value for $M_{\text{dyn}}^{\text{bin}}/M_{\text{dyn}}$ to the 10 least least luminous and the 10 most luminous ETGs. However, the advantage of this method is that the impact of ETGs with exceptional $M_{\text{dyn}}^{\text{bin}}/M_{\text{dyn}}$ on the estimates of the typical $M_{\text{dyn}}^{\text{bin}}/M_{\text{dyn}}$ is minimized.

Note that the effect of binaries on the galactic dynamics is larger in Dabringhausen et al. (2016) than here; especially for low-mass ETGs. The reason for this is that in Dabringhausen et al. (2016), the dynamics predicted by the amount of baryons are taken as the basis, and these defaults are increased by the expected influence that binaries may have. This effect is quite substantial especially for the case of Newtonian dynamics. The least luminous ETGs are expected to have internal velocity dispersions well below 1 km/s in this case, which is by about an order of magnitude lower than $\sigma_{\text{bin}} = 2.3$ km/s. In this paper in contrast, the observed internal velocity dispersions are considered as the default values, and then σ_{bin} is subtracted. The conclusion of Dabringhausen et al. (2016) however, namely that binaries do not increase the dynamical mass enough to substitute the cold dark matter that the ETGs would have according to the Λ CDM-model, becomes even stronger with the approach taken here.

3.7 Rotation

Consider the case of an ETG without binaries, but an average rotation v_{rot} . We furthermore assume that v_{rot} (i.e. ordered motion) and σ_0 (i.e. random motion) are the means of symmetric functions (e.g. Gaussian). The total kinetic energy of the two motions can then be summed up as

$$E_{\text{kin}} = \frac{1}{2} M_{\text{dyn}} \langle v^2 \rangle = \frac{1}{2} M_{\text{dyn}} (\sigma_0^2 + v_{\text{rot}}^2), \quad (31)$$

where $\langle v^2 \rangle$ is the summation over all squared velocities. Thus, in analogy to equation 27,

$$M_{\text{dyn}}^{\text{rot}} = \sqrt{\frac{2 K_V R_e}{G}} E_{\text{kin}} = \frac{K_V}{G} R_e (\sigma_0^2 + v_{\text{rot}}^2) \quad (32)$$

holds for the rotating ETGs.

Fig. 2 shows the ratios of the dynamical masses with and without rotation, i.e. $M_{\text{dyn}}^{\text{rot}}$ over M_{dyn} , plotted over the stellar mass of their galaxies according to the IGIMF-model. The dynamical masses are often substantially higher if also the rotation of the ETGs is considered; sometimes more than twice as high. Only at very low stellar masses,

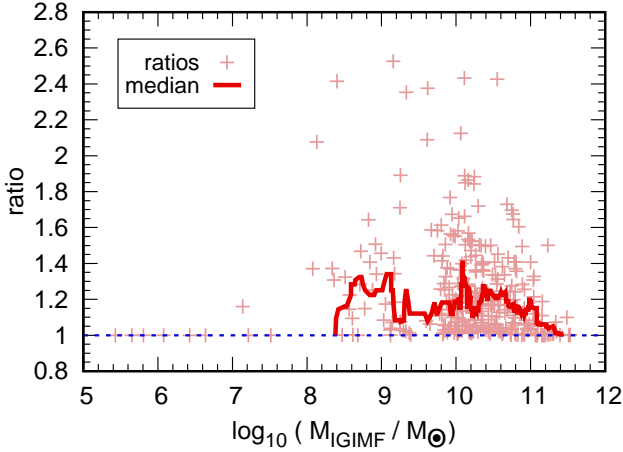


Figure 2. The ratios $M_{\text{dyn}}^{\text{rot}}/M_{\text{dyn}}$ in dependence of M_{IGIMF} for the 310 galaxies of the 462 ETGs in the full sample, for which some estimate of v_{rot} is available. They are shown as light red crosses. The thick dark red line indicates for each galaxy the median value of itself and its 20 closest neighbours in M_{IGIMF} . An Exception are the ten least massive ETGs and the ten most massive ETGs, for which this quantity cannot be calculated, because this quantity should incorporate 10 ETGs with smaller masses and 10 ETGs with larger masses.

the two estimates for the dynamical mass are often the same, but this could also be because rotations are very hard to detect at their luminosities. Also, recall that the estimates of v_{rot} are pretty basic in some ETGs, as described in Dabringhausen & Fellhauer (2016) and Section 2.7.

Also a median, analogously to Fig 1, was calculated in Fig. 2. This median starts at unity for very low stellar masses (see above), and ends at unity for the ETGs with the highest stellar masses, but oscillates from $M_{\text{dyn}}^{\text{rot}}/M_{\text{dyn}} \approx 1.1$ to $M_{\text{dyn}}^{\text{rot}}/M_{\text{dyn}} \approx 1.4$ in between.

Hence, a neglect of the rotation leads to smaller dynamical masses in rotating systems, and thus opposed to the effect of binaries.

3.8 Binaries and rotation

Finally, the effects of binaries and rotation on the dynamical masses of ETGs can also be combined to

$$M_{\text{dyn}}^{\text{bin+rot}} = \frac{K_V}{G} R_e (\sigma_{\text{obs}}^2 - f\sigma_{\text{bin}}^2 + v_{\text{rot}}^2). \quad (33)$$

However, a plot of the ratios of $M_{\text{dyn}}^{\text{bin+rot}}$ over M_{dyn} is next to identical to a plot of $M_{\text{dyn}}^{\text{rot}}$ over M_{dyn} , i.e. Fig. 2. We nevertheless compare $M_{\text{dyn}}^{\text{bin+rot}}$ rather than $M_{\text{dyn}}^{\text{rot}}$ to M_{can} , and M_{IGIMF} , respectively, in Section 4, simply because $M_{\text{dyn}}^{\text{bin+rot}}$ is more comprehensive than $M_{\text{dyn}}^{\text{rot}}$.

3.9 Radial accelerations

When discussing theories of gravity, it is sometimes useful to express the dynamical radial accelerations, a_{dyn} as functions of the prediction for the radial acceleration based on the amount of matter inside the enclosed volume. In Newtonian dynamics and with the assumptions made on ETGs made

in Section 3.5, this is simply

$$a_{\text{dyn}}^{\text{Newt}} = a_{\text{star}}, \quad (34)$$

where the left side of the equation is the dynamical acceleration in Newtonian dynamics, and the right side of the equation is the acceleration due to the stars inside the radius where the dynamical acceleration was measured. The subscript ‘star’ on the left side of the equation signifies that the stellar mass could come from a stellar population with any mass spectrum. Equation 34 is thus the radial acceleration relation (RAR) for Newtonian gravity. It will be referred to as the Newtonian RAR.

The dependency between the two radial accelerations can also be described by the μ -function, which is in the case of Newtonian dynamics given as

$$\mu \left(\frac{a_{\text{dyn}}}{a_0} \right) \times a_{\text{dyn}} = a_{\text{star}}, \quad (35)$$

where a_0 is Milgrom’s constant. This implies

$$\mu \left(\frac{a_{\text{dyn}}^{\text{Newt}}}{a_0} \right) = 1. \quad (36)$$

for the μ -function in Newtonian dynamics.

Things become more interesting in Milgromian dynamics, or MONDian dynamics, where a_0 is the acceleration at the transition between the quasi-Newtonian regime and the deeply Milgromian regime. It is a fundamental constant in Milgromian dynamics, which we set to $1.2 \times 10^{-10} \text{ m s}^{-2}$, in concordance with Famaey & Binney (2005).

In this paper, we pick two μ -functions for Milgromian dynamics, because they are simple, and widely used to date.

The first Milgromian μ -function is the standard μ -function, which was introduced by Milgrom (1983a) as

$$\mu \left(\frac{a_{\text{dyn}}^{\text{std}}}{a_0} \right) = \frac{a_{\text{dyn}}^{\text{std}}}{a_0} \left[1 + \left(\frac{a_{\text{dyn}}^{\text{std}}}{a_0} \right)^2 \right]^{-\frac{1}{2}}, \quad (37)$$

and implies, in combination with equation (35) and solving it for $a_{\text{dyn}}^{\text{std}}$,

$$a_{\text{dyn}}^{\text{std}} = a_{\text{star}} \left(\frac{1}{2} + \frac{1}{2} \left[1 + \left(\frac{2a_0}{a_{\text{star}}} \right)^2 \right]^{\frac{1}{2}} \right)^{\frac{1}{2}} \quad (38)$$

for the RAR. This theoretical RAR will be referred to as the standard-MOND RAR.

Another possible choice for the μ -function is, according to Famaey & Binney (2005) and Zhao & Famaey (2006), the simple μ -function, which is given as

$$\mu \left(\frac{a_{\text{dyn}}^{\text{spl}}}{a_0} \right) = \frac{a_{\text{dyn}}^{\text{spl}}}{a_0} \left[1 + \left(\frac{a_{\text{dyn}}^{\text{spl}}}{a_0} \right) \right]^{-1} \quad (39)$$

and implies in combination with equation (35)

$$a_{\text{dyn}}^{\text{spl}} = a_{\text{star}} \left[\frac{1}{2} + \frac{1}{2} \left(1 + \frac{4a_0}{a_{\text{star}}} \right)^{\frac{1}{2}} \right] \quad (40)$$

for the RAR. This theoretical RAR will be referred to as the simple-MOND RAR.

Note that high-precision measurements at the accelerations in the Solar system formally exclude both functions to different degrees (Blanchet & Novak 2011; Hees et al.

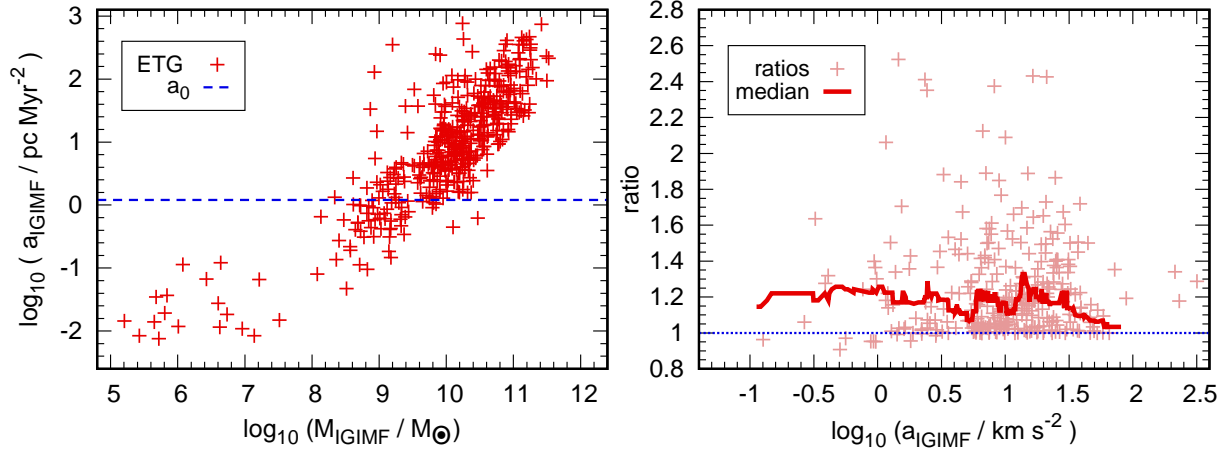


Figure 3. Left panel: The stellar radial accelerations, a_{IGIMF} , in dependence of the stellar masses, M_{IGIMF} , of the 462 ETGs in the full sample calculated with equation 11. High values for a_{IGIMF} are strongly correlated to high values in M_{IGIMF} . Right panel: The ratios $M_{\text{dyn}}^{\text{bin+rot}}/M_{\text{dyn}}$ in dependence of a_{IGIMF} for the 310 galaxies of the 462 ETGs in the full sample, for which some estimate of v_{rot} is available. They are shown as light red crosses. Note that $M_{\text{dyn}}^{\text{bin+rot}}$ is almost equal to $M_{\text{dyn}}^{\text{rot}}$ on the y-axis, and thus a comparison to Fig. 1 essentially only shows the rearrangement of the data by switching from M_{IGIMF} to a_{IGIMF} on the x-axis. The thick dark red line indicates for each ETG the median value of itself and its 20 closest neighbours in a_{IGIMF} . An exception are the ten ETGs with the lowest values in a_{IGIMF} and the ten ETGs with the highest values in a_{IGIMF} , for which this quantity cannot be calculated, because this quantity should incorporate 10 ETGs with smaller radial accelerations and 10 ETGs with larger radial accelerations. In both panels, the mass of the stellar-mass BHs is based on equation 19 and the metallicity the ETGs have today.

2016). However, for the typical accelerations at the half-mass radii of galaxies, which are much lower, they are both fine, with a possible lead for the simple μ -function (e.g. Famaey & Binney 2005; Gentile et al. 2011; Milgrom 2012; Janz et al. 2016; Chae et al. 2019).

There are many more subtly different shapes for $\mu(a_{\text{dyn}}/a_0)$ discussed in the literature, since the correct formulation of $\mu(a_{\text{dyn}}/a_0)$ does to date not follow from Milgromian dynamics itself. For instance, the μ -function introduced by McGaugh (2008) is consistent with the observations in the Solar system, but is difficult to solve for a . However, our main concern here is that the μ -function correctly describes the data in the range relevant to this paper, where the μ -function by McGaugh (2008) closely resembles the simple μ -function. Thus, nothing new would be added by considering it as well.

The next step is to compare these theoretical RARs with observational accelerations in galaxies, as discussed by e.g. Wu & Kroupa (2015), McGaugh et al. (2016) or Lelli et al. (2017). The mass of the galaxy inside the radius where the observation took place, i.e. where the matter responsible for its dynamics is contained, is at least to some extent based on models and assumptions (such as virial equilibrium, the mass-to-light ratio of the stellar population, the presence of a CDM-halo, and so on). If the underlying model of a given theoretical RAR fully accounts for the properties of the considered ETGs, the data on the ETGs will be located along the respective theoretical RAR. However, agreement between the data and the theoretical RAR is not a sufficient condition for the underlying assumptions to be correct, while a systematic deviation from the theoretical RAR indicates for a certainty that some of the made assumptions are wrong, or some important aspect is missing in the models for the ETGs.

In principle, a RAR can be tested on many differ-

ent radii of the same galaxy. However, here we test every galaxy only once at its half-mass radius R_{h} , which is derived according to the assumptions made in Section 3.5. Moreover, according to the appendix in Wolf et al. (2010), $R_{\text{h}} \approx (4/3) R_e$. This is remarkably independent of the mass profile actually used to model the ETG or the star cluster. Thus,

$$a_{\text{dyn}}^{\text{obs}} = \frac{1}{2} \frac{G M_{\text{dyn}}^{\text{obs}}}{R_{\text{h}}^2} \approx \frac{9}{32} \frac{G M_{\text{dyn}}^{\text{obs}}}{R_e^2} \quad (41)$$

for the observed radial acceleration.

The corresponding predicted stellar radial acceleration to $a_{\text{dyn}}^{\text{obs}}$ is in this paper

$$a_{\text{IGIMF}} = \frac{1}{2} \frac{G M_{\text{IGIMF}}}{R_{\text{h}}^2} \approx \frac{9}{32} \frac{G M_{\text{IGIMF}}}{R_e^2}, \quad (42)$$

where M_{IGIMF} is the stellar mass. Multiplication of equation 42 with the according μ -function would give the prediction of the dynamical radial acceleration at this stellar radial acceleration; e.g. equations 36, 37 and 39 for the choices in this paper.

The dependency between stellar radial relations, a_{IGIMF} , and stellar mass, M_{IGIMF} , is illustrated in Fig. 3 for the specific case of the simplified IGIMF (equation 11). In the left panel of Fig. 3, high values in a_{IGIMF} are clearly strongly correlated with high values in M_{IGIMF} . This is not obvious. Imagine two ETGs, which have the same stellar mass, but different half-mass radii. The radius shall be much larger in the second ETG than in the first ETG, so that the first ETG will have a larger stellar radial acceleration at its half-mass radius. However, in reality, the rise of the average radii with luminosity, or mass (see figure 2 in Dabringhausen & Fellhauer 2016) is not strong enough to negate or reverse the trend of rising accelerations with rising luminosity, or mass. In the right panel of Fig. 3, the ratios

of $M_{\text{dyn}}^{\text{bin+rot}}/M_{\text{dyn}}$ are plotted over their stellar radial accelerations. Also the medians of $M_{\text{dyn}}^{\text{bin+rot}}/M_{\text{dyn}}$ are shown as a (red) solid line. They are created as in Fig. 1, but based on the stellar radial accelerations instead of their stellar masses. The right panel of Fig. 3 can thus be compared to Fig. 2, which shows essentially the same data on the y-axis (see the discussion on $M_{\text{dyn}}^{\text{rot}}$ and $M_{\text{dyn}}^{\text{rot+bin}}$ in Section 3.8 of the present paper), but with stellar masses instead of the stellar radial accelerations on the x-axis.

4 RESULTS

4.1 ETGs with the canonical IMF

Fig. 4 shows the data on the dynamical radial accelerations of the 462 ETGs in our sample over their stellar radial accelerations. All ETGs are assumed here to have formed with the canonical IMF; i.e. without the changing IMFs according to the IGIMF-model. Also the effect of binaries, or that many of the ETGs also rotate, is not considered in the estimates of a_{dyn} . The data are compared to the Newtonian RAR (equation 34), the standard-MOND RAR (equation 38), and the simple-MOND RAR (equation 40). If one of these RARs encodes the dynamics of ETGs correctly, the data for the observed ETGs should be located along it. This is definitely not the case for the Newtonian RAR, which lies below most of the data. This is by orders of magnitude for low-mass ETGs with radial accelerations below the critical acceleration, a_0 . Much of the data also lie above the Milgromian RARs, even though this is particularly at $a_{\text{can}} < a_0$ much alleviated compared to the Newtonian RAR. Thus, unless non-baryonic dark matter is introduced, the data calls either for additional physical laws, for a decrease of the dynamical mass or an increase of the stellar mass including the stellar remnants of the ETGs. In old stellar systems like in the present sample, the latter can be the consequence of an overabundance of low-stars, an overabundance of high-mass stars, or both, compared to the canonical IMF.

The concept behind thin solid thin curves is the same as of the thick solid red line, except that they do not show the position of the ETGs with the eleventh-most a_{dyn} in their samples of 21 ETGs with neighbouring a_{dyn} , i.e. their medians. Instead, they indicate the ETGs with the fourth-most a_{dyn} , and the 18th-most a_{dyn} , respectively. Alternatively, the lower green line is approximately the 16th percentile of ETGs with lower a_{dyn} , the thick red line the 50th percentile, and the upper green line the 84th percentile. Thus, the two green lines indicate approximately the variance of the a_{dyn} of the sample of ETGs. However, this variance is not necessarily equal to the uncertainty of the measurements, but can in part be a real property of the sample itself. In other words, it is possible that not all of the variance would not go away, even if the errors to the measurements were infinitesimally small.

Fig. 5 shows a subset of 310 ETGs of the sample of 462 ETGs plotted in Fig. 4, for which $M_{\text{dyn}}^{\text{bin+rot}}$ instead of M_{dyn} is shown on the y-axis. The data on the x-axis remains with a_{can} for every ETG the same as in Fig. 4. However, the binary stars have almost no effect on M_{dyn} (see Section 3.6), and the rotation of the ETGs still increases the mass needed to keep the ETGs in dynamical equilibrium. In other words,

the disagreement of the data to the theoretical predictions from the RARs is even stronger than in Fig. 4. On the other hand, rotation definitely takes place in many of the ETGs, even though its effect in Fig. 5 should perhaps be taken as an upper limit (see Section 3.7). The most realistic values for the dynamical masses of the ETGs lie therefore probably in between the values shown in Fig. 4 (lower limit) and Fig. 5 (upper limit).

4.2 ETGs with the IGIMF

In contrast to Section 4.1, where the stellar radial accelerations of the ETGs were based on the canonical IMF (equation 1), they are in this Section based on the simplified IGIMF (equation 11; Section 3.2).

As in Section 3.5, the ETGs are separated in those with central velocity dispersions $\sigma_0 \leq 100$ km/s and those with $\sigma_0 > 100$ km/s.

For the ETGs with $\sigma_0 > 100$ km/s, the procedure of finding their IGIMF described in Sections 3.1 to 3.4 is applied only where equation 21 produces values $\Upsilon > \Upsilon_{\text{can}}$, i.e. only for radii $R \leq 0.388R_e$. The parameters in equation 21 are for $\epsilon = 1.29$ and $\eta = 3.33$. For radii $R > 0.388R_e$, the IGIMF corresponds to the canonical IMF, indicating a moderate star formation like in the Milky Way there.

For ETGs with $\sigma_0 \leq 100$ km/s, the recipe for finding their IGIMF is applied throughout the whole ETGs, without any radius restrictions.

Following the notion that the SFR follows matter density, the SFR should be changing within an ETG with radius, and consequently should its IGIMF. The ETGs with $\sigma_0 \leq 100$ km/s are also those which have $M_{\text{IGIMF}} \lesssim 5 \cdot 10^9 M_{\odot}$, and as such they have high-mass IGIMF-slopes $\alpha_{\text{IGIMF}} \gtrsim 2.3$ (see Dabringhausen 2019). The mass difference between the two extreme cases, namely an ETG that has $\alpha_{\text{IGIMF}} = 2.3$ up to $150 M_{\odot}$ and the same ETG with a mass cutoff above $1 M_{\odot}$ is about 20 percent. Consequently, the errors made by assuming a constant IGIMF instead of a varying one are comparatively small in this range.

However, for $M_{\text{IGIMF}} > 5 \cdot 10^9 M_{\odot}$, the mass gain with rising galaxy mass is increasingly fast compared to a canonical IMF. It might reach values of ≈ 2 for the most massive ETGs, if the IGIMF in their outskirts was the same as in their centres (see figures 8 and 9 in Dabringhausen 2019). Thus, allowing for a change in the IGIMF with radius is much more important for high-mass ETGs, and the overall increase in mass drops from $M_{\text{IGIMF}}/M_{\text{can}} \approx 2$ to $M_{\text{IGIMF}}/M_{\text{can}} \approx 1.4$.

In Fig. 6, the masses of the stellar-mass black holes are thought to be influenced by the metallicities that the ETGs have today. They are given by equation 19. The masses of the stellar-mass BHs become especially important in the high-mass ETGs, which had high SFRs, and therefore top-heavy IGIMFs. Thus, they have many stellar-mass BHs, compared to ETGs with the canonical IMF. The binaries and the rotation of the ETGs is neglected in Fig. 6. The high-acceleration, and thus predominately high-mass ETGs fit much better to the theoretical Milgromian RARs in Fig. 6 than in Figs. 4 and 5, where the star formation in the ETGs took place with the canonical IMF.

Fig. 7 considers also the binaries and the rotations of the ETGs (see Sections 3.6 and 3.7), in contrast to Fig. 6.

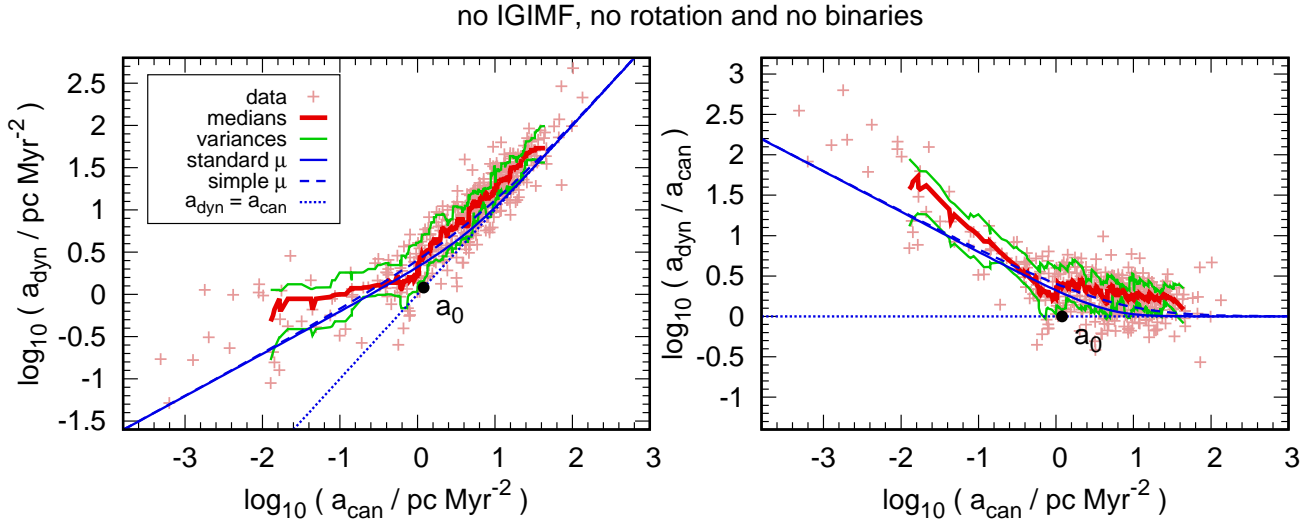


Figure 4. Left panel: The radial accelerations for ETGs without accounting for the IGIMF. On the x-axis is the expected acceleration based on the amount of baryons present in the ETGs under the assumption of Newtonian dynamics, a_{can} . On the y-axis is the acceleration implied by the observed dynamics under the assumption of virial equilibrium, a_{dyn} . The thin light red crosses show the data for the individual ETGs. The thick dark red line is for each galaxy the median in a_{dyn} of itself and its 20 closest neighbours in a_{can} . An Exception are the ten ETGs with the lowest value in a_{can} and the ten ETGs with the highest value in a_{can} , for which this quantity cannot be calculated, because this quantity should incorporate 10 ETGs with smaller radial accelerations and 10 ETGs with larger radial accelerations. The concept of the solid green lines is the same of the thick red line, except that they do not indicate the median, but the location of the fourth most massive galaxy, and fourth least massive galaxy, respectively, of their samples of 21 neighbouring ETGs in a_{dyn} . The thin blue lines represent the different RARs discussed in this paper: the dotted blue line stands for Newtonian dynamics, the dashed blue line stands for Migromian dynamics with the simple μ -function and the solid blue line stands for Migromian dynamics with the standard μ -function. Right panel: The same as the left panel, but with $\log_{10}(a_{\text{dyn}}/a_{\text{can}})$ on the y-axis. This rescaling makes the offset between the data and the theoretical predictions better visible. In both panels, the mass of the stellar-mass BHs is based on equation 19 and the metallicity the ETGs have today.

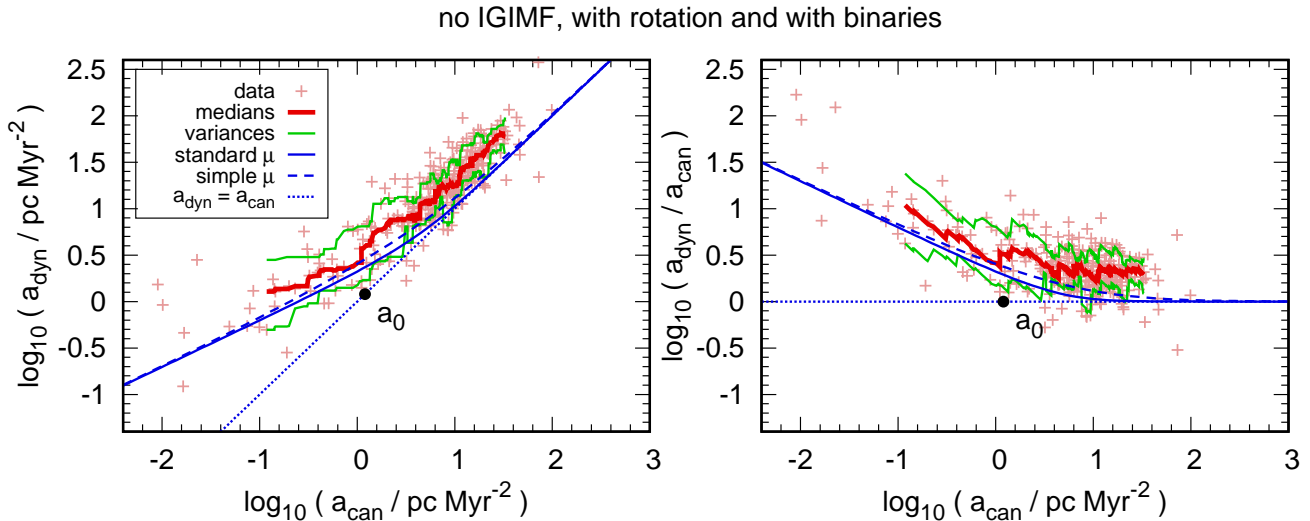


Figure 5. As Fig. 4, but with the dynamical accelerations of the ETGs adjusted for the presence of rotation and binaries in them.

All other parameters are the same as in Fig. 6. Compared to Fig. 6, considering rotation therefore increases the dynamical radial accelerations needed to keep the ETGs in equilibrium, and thus the dynamical masses. In the end, the values for a_{dyn} are too high on average here as well, except for the ETGs with the highest a_{dyn} . Due to the close correlation between masses and accelerations of the ETGs (see left panel of Fig. 3), this can be translated into a deficiency of M_{dyn}

with growing M_{IGIMF} for ETGs with $M_{\text{IGIMF}} \geq 10^{11} M_{\odot}$, to the point where $M_{\text{IGIMF}} > M_{\text{dyn}}$ on average. In contrast to $M_{\text{IGIMF}} < M_{\text{dyn}}$, which could be explained by undetected matter, $M_{\text{IGIMF}} > M_{\text{dyn}}$ indicates an overestimate of matter with our model in the most massive ETGs (see especially the end of this Section for an explanation).

It is likely however that the metallicities the ETGs have today are higher than the metallicities under which most of

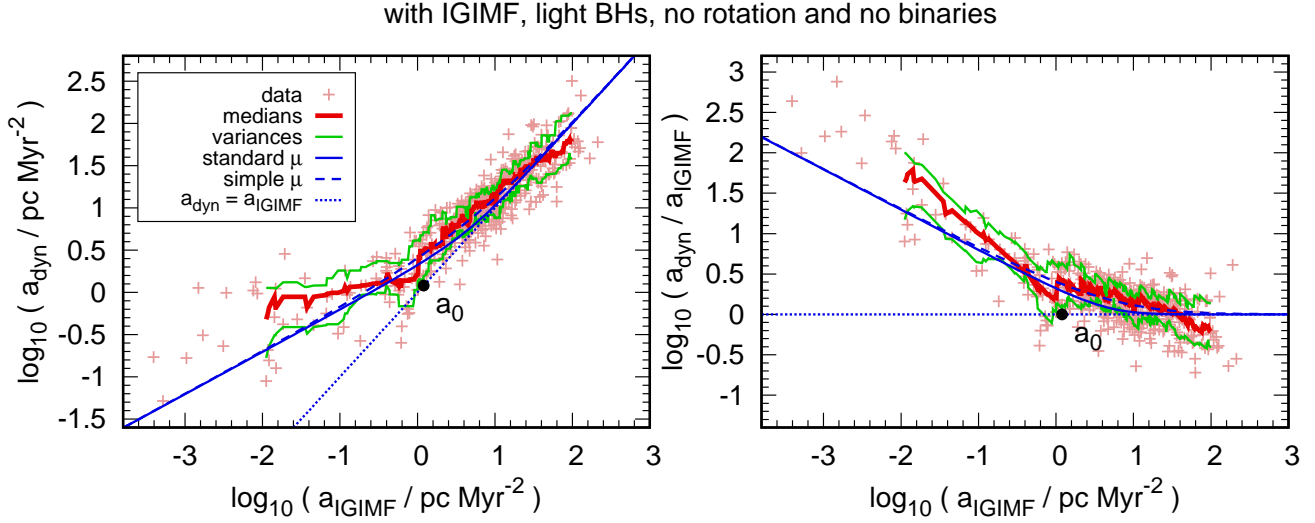


Figure 6. As Fig. 4, but with the stellar radial accelerations adjusted to the IGIMF (Sections 3.1 to 3.4) instead of using the canonical IMF (equation 1) for star formation in every ETG. The masses of the stellar-mass BHs follow equation 19 for the metallicities that the ETGs have today. Note that binaries and rotation of the ETGs are *not* considered.

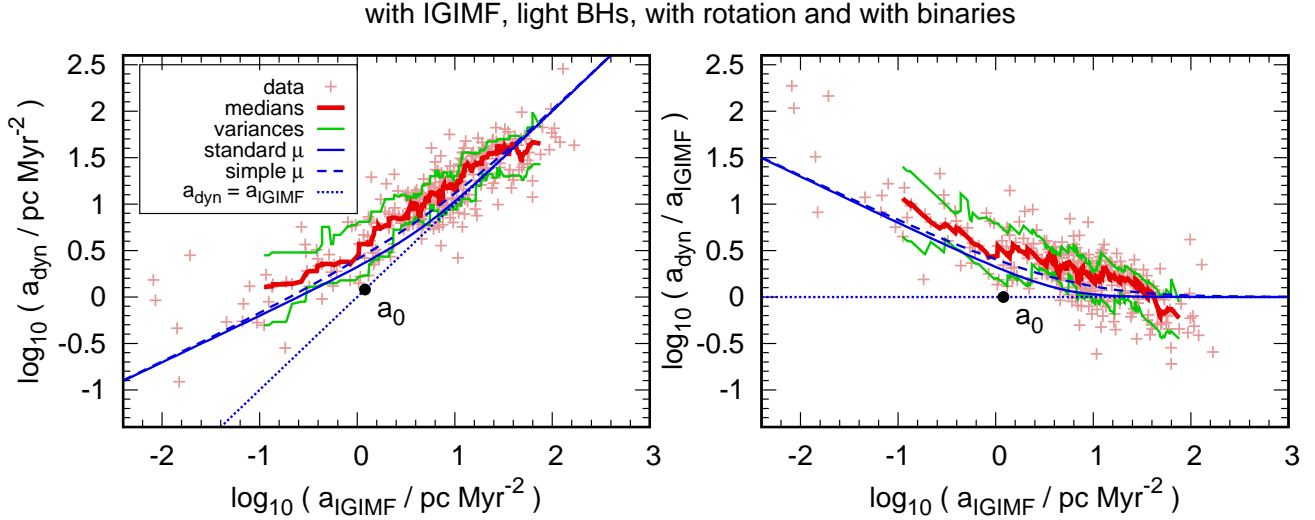


Figure 7. As Fig. 6, but with the dynamical accelerations of the ETGs adjusted for the presence of rotation and binaries in them.

the star formation in the massive ETGs took place. This is not modelled in this paper, but convincingly shown in Figure 2 in Jeřábková et al. (2018). The masses of the stellar-mass BHs depend on the metallicities of the progenitor stars in such a way, that the more metal-poor the progenitor star is, the more massive the stellar-mass BH evolving out of it becomes; see e.g. figures 12 and 16 in Woosley et al. (2002). These figures are however very imprecise, and only allow to name this general trend. What can be said though is that equation 19 most likely underestimates the real masses of stellar-mass BHs, even though it is only a very rough estimate by itself. Thus, we show in Figs. 8 and 9 also the results for the ETGs with the simplified IGIMF for the stellar-mass BHs having the initial mass of their progenitor stars. This is a strict upper limit, because real metal-poor massive stars also have stellar winds, albeit much less than their metal-rich counterparts.

Fig. 8 shows the data without considering binaries and rotation of the ETGs. Fig. 9 is the same as Fig. 8, except that also the rotation and the binaries of the ETGs are considered. Thus, the data shown here are arguably more realistic than in Fig. 8.

Fig. 10 shows the ETGs in terms of dynamical masses versus stellar masses instead of accelerations. The ETGs in this figure are plotted without considering rotation or binaries, and the masses of the stellar-mass BHs are roughly sketched based on the average metallicities that the ETGs have today. For the IGIMF-model with the assumptions made in this paper, the curve indicating the medians of the ETGs flattens in M_{dyn} for $M_{\text{IGIMF}} \gtrsim 10^{10} M_{\odot}$. For the ratios between M_{dyn} and M_{IGIMF} , the curve goes downwards on average with increasing M_{IGIMF} until it nearly reaches $M_{\text{dyn}}/M_{\text{IGIMF}} = 1$ at $M_{\text{IGIMF}} \approx 10^9 M_{\odot}$, then has upwards tendency for $10^9 M_{\odot} \lesssim M_{\text{IGIMF}} \lesssim 10^{10} M_{\odot}$, and

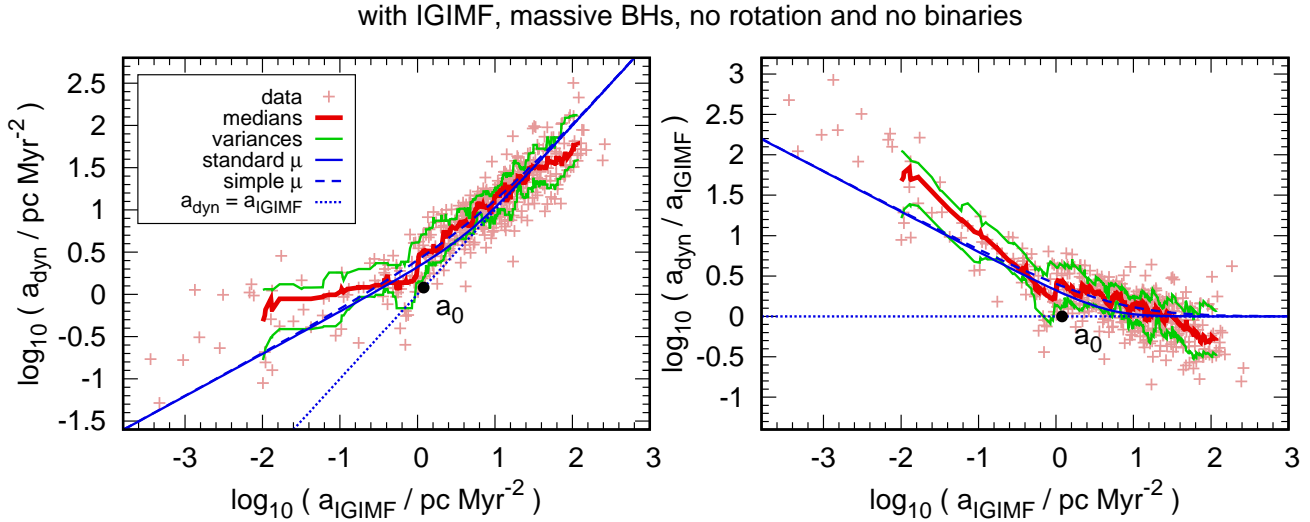


Figure 8. As Fig. 6, but with the masses of the stellar-mass BHs set to the initial mass of their progenitor stars, instead of that their masses follow equation 19 and the metallicities are as measured today. Note that binaries and rotation of the ETGs are *not* considered.

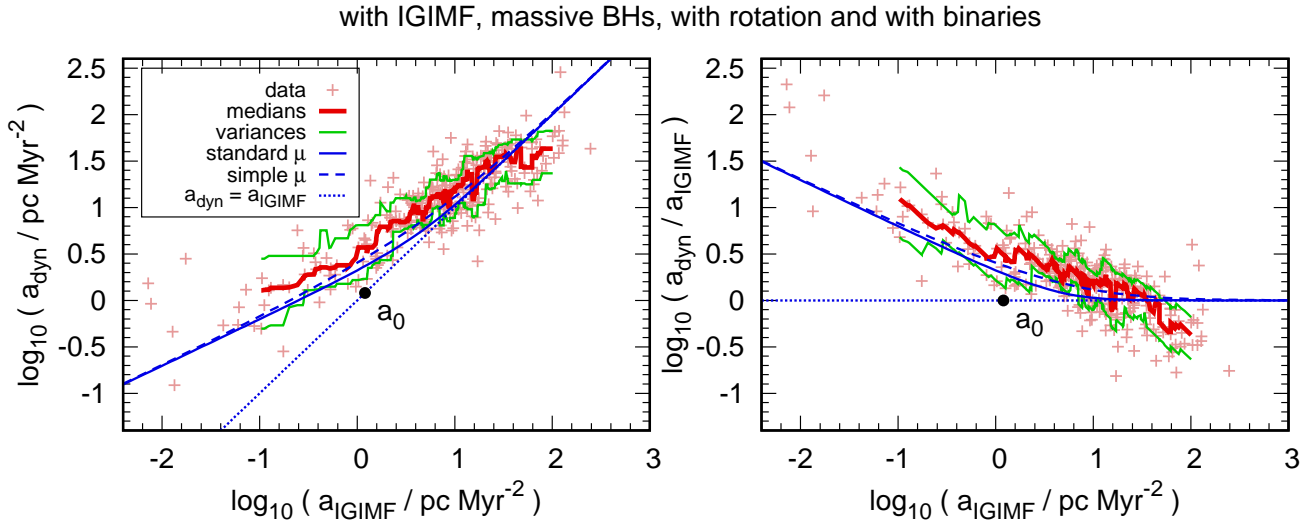


Figure 9. As Fig. 8, but with the dynamical accelerations of the ETGs adjusted for rotation and presence of binaries in them.

continues its downwards trend for $M_{\text{IGIMF}} \gtrsim 10^{10} M_{\odot}$. For $M_{\text{IGIMF}} \gtrsim 10^{11} M_{\odot}$, $M_{\text{dyn}} < M_{\text{IGIMF}}$.

The last point indicates that the IGIMF-model, as it is applied here, very likely overestimates the mass in stars and stellar remnants for $M_{\text{IGIMF}} \gtrsim 10^{11} M_{\odot}$, because the ETGs cannot have $M_{\text{dyn}} < M_{\text{IGIMF}}$ systematically. It is not certain, however, whether such massive objects form in a single collapse, or rather as a merger of several smaller galaxies, as described e.g. in De Lucia & Blaizot (2007) for the most massive ETG in the centres of galaxy clusters in the Λ CDM-model, or Eappen et al. (2022) for the same in an Milgromian model. The dynamical masses of smaller galaxies do not undercut their stellar masses as severely, or may even be larger than the stellar masses, even in the simple model presented here.

4.3 Star formation times

The SFRs of the ETGs can be calculated based on the star formation times from Yan et al. (2021), and the mass derived from the stellar content of the ETGs, M_{IGIMF} . Yan et al. (2021) have calculated the star formation times for ETGs with $M_{\text{can}} < 5 \cdot 10^9 M_{\odot}$ themselves, but above this mass limit, the star formation times are the ones from McDermid et al. (2015). The median values are shown as equations 18 and 19 in Yan et al. (2021), or equation 16 here. However, even though M_{IGIMF} is the mass created through star formation according to the IGIMF, is not necessarily equal to M_{dyn} , which is the dynamical mass of the ETG. Especially for the more massive ETGs, which are not easily disturbed by tidal fields, M_{dyn} indicates the total amount of matter a ETG contains. If the ETGs formed with the IGIMF and with the calculated SFR, but without non-baryonic DM, then their star formation times should be as long as

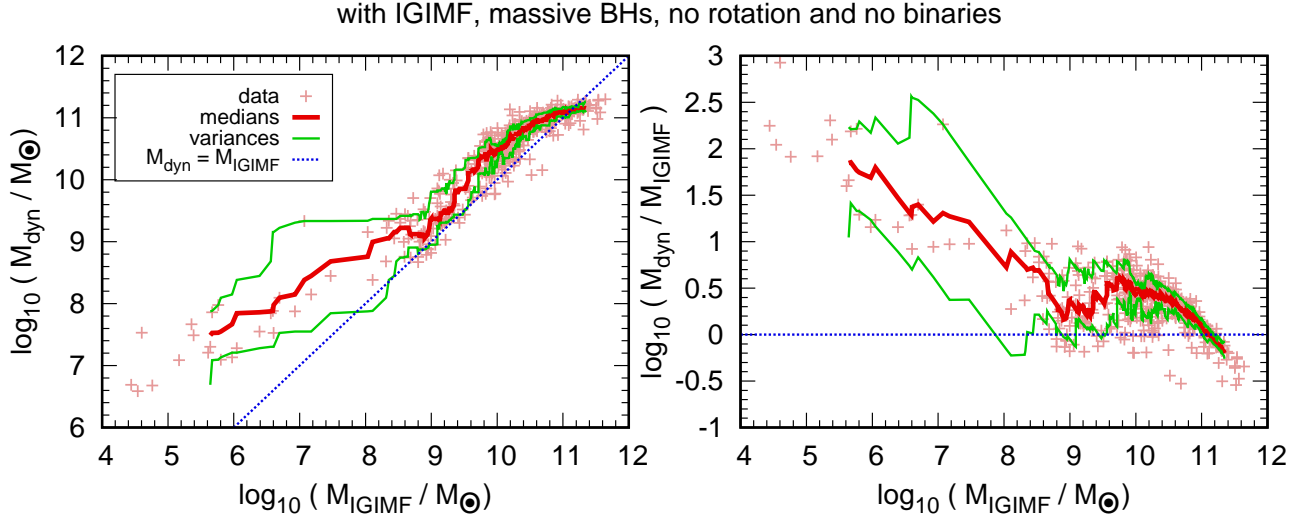


Figure 10. The dynamical masses over their stellar masses for the ETGs in the IGMF-model. Rotation and binary stars are not included here, and the masses of stellar-mass BHs equal the initial masses of their progenitor stars. The thick solid red curves are the medians of the ETGs. The thin solid green lines indicate the position of the ETGs with fourth-most M_{dyn} , and 18th-most M_{dyn} , respectively, in samples of 21 ETGs with neighbouring M_{dyn} . Their concept is thus similar to the thick solid red curves, except that the red curves show the position in M_{dyn} of the ETGs with the eleventh-most M_{dyn} . The dotted (blue) lines indicate equality between the two mass estimates.

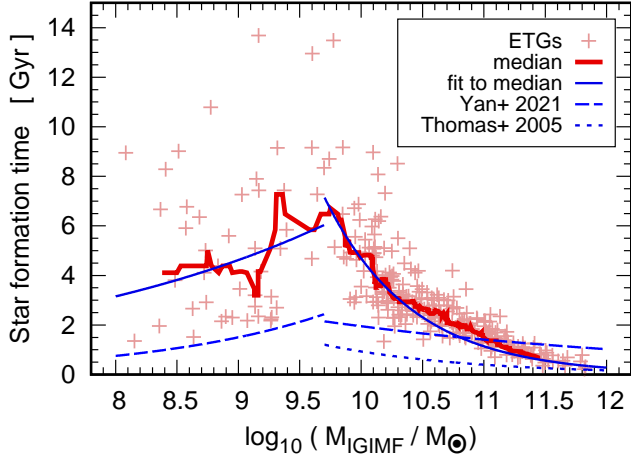


Figure 11. The star formation times of the ETGs with $a/a_0 > 0.1$. Shown is the time it takes for the ETGs to reach their M_{dyn} with the star formation rate as calculated from equation 16 as thin light red crosses. The thick dark red line is for each galaxy the median in M_{dyn} of itself and its 20 closest neighbours in M_{can} . An exception are the ten ETGs with the lowest value in M_{can} and the ten ETGs with the highest value in M_{can} , for which this quantity cannot be calculated. This is because this quantity should incorporate 10 ETGs with even smaller M_{can} , and 10 ETGs with even larger M_{can} , respectively. The solid blue curve is the data for the ETGs fitted with equation 43 for $M_{\text{IGIMF}} \leq 5 \cdot 10^9 M_{\odot}$ (i.e. the breaking point of the curve), and the same equation with a different set of parameters for $M_{\text{IGIMF}} > 5 \cdot 10^9 M_{\odot}$. It has thus the same functional structure like the dashed blue curve, but different parameters. The dashed blue curve traces equation 16, and approximates the time it takes for the ETGs to reach their M_{IGIMF} with their SFR according to Yan et al. (2021). Equation 16 is equal to equation 3 in McDermid et al. (2015) for $M_{\text{IGIMF}} > 5 \cdot 10^9 M_{\odot}$. Also equation 5 from Thomas et al. (2005) is shown for comparison as dotted blue curve.

it takes for them to reach M_{dyn} . These star formation times are shown in figure 11 for ETGs with $a/a_0 > 0.1$. Also shown in this figure is a least-squares fit of these data with

$$F(M_{\text{IGIMF}}) = \beta (M_{\text{dyn}}/M_{\odot})^{\gamma}. \quad (43)$$

It is shown as a solid blue line in Fig. 11. For $M_{\text{IGIMF}}/M_{\odot} \leq 5 \cdot 10^9 M_{\odot}$, the parameters β and γ in Equation 43 are $\beta = 0.148 \pm 0.135$ and $\gamma = 0.166 \pm 0.036$. For $M_{\text{IGIMF}}/M_{\odot} > 5 \cdot 10^9 M_{\odot}$, they are $\beta = 5.50 \cdot 10^5 \pm 0.79 \cdot 10^5$ and $\gamma = -0.507 \pm 0.006$.

It is actually not important for the parameters found for Equation 43 which one of the two extreme choices regarding the mass of the stellar-mass BHs introduced in Section 3.4 are made. These are (1) an estimate of the BH-masses inspired by the metallicities that the ETGs have today and (2) assuming the initial mass of the progenitor stars for the BH mass. The parameters actually given in equation 43 are for the arithmetic means of the two extremes. For all other parameter choices, the deviation is $\lesssim 10^{-3}$ times the values given for Equation 43, or in other words, less than the line width of the solid curve in figure 11.

Also equation 16 is shown in this figure as a dashed blue line, which is where the SFRs, on which equation 43 is based, originate. Thus, equation 43 is not a completely independent estimate of the star formation times of the ETGs. Instead, if the star formation rate of an ETG would be given, then equation 16 would give the time it would take the ETG to reach M_{IGIMF} , and equation 43 would give the time it would take the same ETG to reach M_{dyn} . Equation 16 is also the best fit to the data from GALIMF in Yan et al. (2021). Finally, equation 5 from Thomas et al. (2005) is shown for comparison.

For estimating the difference between M_{IGIMF} and M_{dyn} , the simple μ -function was taken, as it probably represents the data in the acceleration range of ETGs better than the standard μ -function (e.g. Milgrom 2012; Chae et al.

2019). ETGs with $a/a_0 < 0.1$ were omitted, because they probably suffer from tidal distortions to a large amount (see figures 4 to 9).

In essence, equation 43 is an estimate for the star formation times of the ETGs, based on their measured masses of the ETGs according to their dynamics. This approach confirms downsizing, i.e. less massive ETGs formed less rapidly. Incidentally, downsizing appears to be a consequence of the formation of ETGs through direct free-fall gravitational collapse of non-rotating gas clouds in the Milgromian framework (Eappen et al. 2022).

5 DISCUSSION

In summary, the Newtonian theoretical RAR does not fit to the observations of the ETGs in any of the Figs. 4 to 9. Especially in the low-acceleration part, the deviance of the Newtonian RAR and the observations is extreme. Many authors have tried to solve this issue before by adding non-baryonic dark matter to the ETGs. For low-luminosity ETGs, corresponding mainly to low radial accelerations, this has been done for e.g. by Strigari et al. (2008); Wolf et al. (2010) and Ackermann et al. (2014). For high-luminosity ETGs, corresponding mainly to high radial accelerations, this has been done for instance by Cappellari et al. (2006); Bolton et al. (2008) and Tortora et al. (2009). A slightly better fit is achieved for the high-luminosity ETG with the Milgromian theoretical RARs. Both Newtonian dynamics and Milgromian dynamics do however need the IGIMF-theory (or something equivalent) to fit the data in the high-luminosity range.

It is striking that $M_{\text{dyn}} < M_{\text{IGIMF}}$ on average for the highest values of M_{IGIMF} . This could point to the simplicity of the model proposed here. For instance, it is assumed here that all ETGs formed in a similar fashion, independent of their mass. In truth however, the low-mass ETGs might form through monolithic collapses, while the most massive ETGs might form by mergers. The IGIMFs of the most massive ETGs would thus be more akin to their less massive counterparts than proposed here, because they were formed from such. Also, Fig. 11 shows the variety of parameters that different teams find in fitting an exponential function to the data of the star formation times of ETGs in dependence of their mass. However, even choosing an exponential function for this task was an ad-hoc choice in the first place. Moreover, the metallicity dependence was completely neglected in the model proposed here.

For extremely low radial accelerations, the ETGs tend to have higher dynamical radial accelerations than also the theoretical Milgromian RARs suggest. This discrepancy is however still lower of the order of one or two magnitudes than in Newtonian dynamics.

We will discuss these problems in the next Sections.

5.1 Out-of-equilibrium dynamics

Out-of-equilibrium dynamics could well be the reason for extremely high mass-to-light ratios in ETGs (Kroupa 1997; Casas et al. 2012).

However, the high-mass ETGs have mainly also large accelerations (left panel of Figure 3), and are therefore hard to disturb by external gravitational fields. This is not

to say that it cannot be done, as examples of mergers of massive galaxies show (e.g. Toomre 1977). Even if they were ETGs and in equilibrium before, they are irregular galaxies out of equilibrium during the interaction process. They are therefore unlikely to appear in the catalogue by Dabringhausen & Fellhauer (2016), or in this paper, even though they will eventually become ETGs. Thus, the high-mass ETGs in this paper can safely be assumed to be in virial equilibrium, and their elevated mass-to-light ratios must have other reasons (like the IGIMF discussed here).

The low-mass ETGs on the other hand, i.e. predominantly the ETGs with luminosities $L_V \lesssim 10^6 L_\odot$, are very easy to disturb by external gravitational fields. This is because also their radial accelerations are low (left panel of Figure 3). The traces of these disturbances are tidal streams, which are however hard to detect because they are very faint, in contrast to the tidal streams of their more massive counterparts. Thus, low-mass ETGs are not necessarily excluded from the catalogue by Dabringhausen & Fellhauer (2016), because Dabringhausen & Fellhauer (2016) decided on the appearance of the galaxy as an ETG (i.e. no clear tidal streams detected), and their classification as ETGs in the source literature. Also recall that low-mass ETGs, just as their more luminous counterparts, contain little gas (Mateo 1998)². Thus, gas in general cannot be the reason for their high dynamical radial accelerations.

There is strong evidence that many, if not most low-mass ETGs are tidal dwarf galaxies (e.g. Kroupa et al. 2010; Dabringhausen & Kroupa 2013; Haslbauer et al. 2019) and are as such basically free of non-baryonic dark matter (e.g. Barnes & Hernquist 1992b; Bournaud 2010). At least in the Λ CDM-model (and thus Newtonian dynamics), low-mass, dark-matter-free systems are vulnerable to tidal forces, as opposed to systems which are protected by the mass of their surrounding CDM-haloes (Smith et al. 2015). Tidal forces can thus increase the internal velocity dispersions of tidal dwarfs by additional pulls from the outside. Consequently, the estimates for the mass of the object is elevated if the (in this case wrong) assumption of tidal equilibrium is held (Kroupa 1997; Casas et al. 2012; Domínguez et al. 2016). Even a system disrupted by tides may still be detected as an over-density of stars, for which σ_{obs} and R_e can be observed. However, an estimate of the mass of the system based on equations 24, 29, 32 or 33 is clearly impossible. Also interactions with intergalactic gas may drive low-mass ETGs out of virial equilibrium (Yang et al. 2014).

Besides their (at least apparently) high mass-to-light ratios, there is also other evidence that low-mass ETGs are tidally disturbed. For instance, the ETGs around the Milky Way are generally more elliptical, the less massive and the closer to their host galaxy they are (McGaugh & Wolf (2010)). More detailed observations of single galaxies show further peculiarities that can be interpreted as evidence for non-equilibrium dynamics for many of these ETGs, like elongated or irregular shapes, asymmetric surface-brightness profiles, or asymmetric velocity-dispersion profiles (e.g. Belokurov et al. 2006, 2007; Walker et al. 2009;

² There is one exception to this rule: The Leo T dSph may contain more gas than stars (Ryan-Weber et al. 2008)

Muñoz et al. 2010; Willman et al. 2011; Deason et al. 2012; Asencio et al. 2022).

Thus, assuming Milgromian dynamics for low-mass ETGs implies that some of them are probably disturbed by tidal fields, but not necessarily all of them, as can be seen in Figs. 4 to 9. This scenario appears more likely than the case that virtually *all* low-mass ETGs are out of virial equilibrium, as assuming Newtonian dynamics would suggest for them, unless they contain non-baryonic dark matter (Dabringhausen et al. 2016).

Milromian dynamics was incorporated independently by Candlish et al. (2015) and by Lüghausen et al. (2015) into RAMSES by Teyssier (2002). It will be interesting to use these codes to compute the tidal processing of dwarf satellite galaxies in Milgromian dynamics, using the same approach as in Kroupa (1997).

5.2 How symmetric is the data?

How good is the assumption of complete isotropy of the *random* motions in the ETGs in Section 3.5?

If the mass-to-light ratios are constant, the observed line-of-sight velocity distributions of over 2000 ETGs studied by Vudragović et al. (2016) indicate that radial orbits are preferred over tangential orbits in them. Consequently, Vudragović et al. (2016) find for their sample of ETGs that more realistic mass estimates based on the internal dynamics are on average about 10 per cent higher than expected under the assumption of isotropy. The noted discrepancy between mass estimates based on the internal dynamics of ETGs and mass estimates based on the amount of baryons detected in them is usually interpreted as a presence of non-baryonic dark matter.

On the other hand, Chae et al. (2019) have studied slowly rotating, massive ETGs from the ATLAS^{3D}-sample (Cappellari et al. 2011), which are also part of the sample presented here. They have shown that the need for anisotropic velocity dispersions is relaxed, if the mass-to-light ratio increases towards the centres of the ETGs. Moreover, Chae et al. (2019) use exactly the same parametrization of the gradient in the mass-to-light ratio as we do (Section 3.5). Thus, in consequence, assuming that the *random* motion in ETGs is completely isotropic is perhaps not as far from the truth, as it would appear from Vudragović et al. (2016).

6 SUMMARY AND CONCLUSIONS

If massive early-type galaxies (ETGs) formed with the canonical IMF (equation 1) and are in tidal equilibrium, they are generally too massive for their light by a factor of the order of two. There is in principle no reason why alternative stellar mass functions could not be the reason, except for the long-standing paradigm that the canonical IMF is also universal to all star formation (Kroupa 2001). For the missing mass, non-baryonic dark matter is substituted (see e.g. Cappellari et al. 2006; Bolton et al. 2008; Tortora et al. 2009).

Here we propose an alternative by saying that ETGs have formed according to the IGIMF-theory (Jeřábková et al. 2018 and references therein), and they

obey Milgromian Dynamics, or MODified Newtonian Dynamics (MOND) instead of Newtonian Dynamics. Finally, also the assumption of virial equilibrium might have to be relaxed in them. To do this, the ETGs are plotted with their observed dynamical accelerations versus their accelerations based on their presumed stellar populations. The results are then compared to different radial acceleration relations (RARs), i.e. predictions for the dynamical radial accelerations as functions of the baryons contained in the galaxies (Wu & Kroupa 2015; McGaugh et al. 2016; Lelli et al. 2017).

This not to say that there were no attempts before to explain the properties of massive ETGs with IMFs different to the canonical one (equation 1). For instance, van Dokkum & Conroy (2010); Ferreras et al. (2013) and La Barbera et al. (2013) had to use IMFs with more faint low-mass stars than the canonical IMF to explain the ratios of line indices in ETGs. The IMFs they proposed were however constant in time and space in each ETG. Later on, the independence of space in an ETG was relaxed by La Barbera et al. (2016); van Dokkum et al. (2017); Parikh et al. (2018) and Sarzi et al. (2018), who detected gradients in the IMFs of the ETGs they observed, such that the overabundance of low-mass stars was tied to the centres of the ETGs, while at their outskirts their IMFs approached the canonical IMF. Leier et al. (2016) confirmed from the line indices of the massive ETGs that they are overabundant in low-mass stars compared to the canonical IMF, while the masses that these slopes suggest are still too light for the masses that gravitational lensing implies.

This puzzle may be resolved with an IMF that can change in space *and* time, like sketched in fig. 2 of Jeřábková et al. (2018) for the IGIMF-model. The IGIMF-model was introduced by Kroupa & Weidner (2003), and further developed for the stellar populations of ETGs by Weidner et al. (2013a) and Weidner et al. (2013b) as a theory where the shape of the IMF depends on the star formation rate (SFR) and the metallicity of the star forming medium. An ETG, which is too massive for its contemporary IMF, can be understood in the IGIMF-model by having a high SFR in its past and therefore formed an overabundance of stars which have become NSs and BHs today, whereas today it is more metal-rich than the Milky Way and thus forms an over-abundance of low-mass stars. In consequence, we measure the light from the stellar population of today, but its total mass is boosted by burnt-out stars instead of non-baryonic dark matter. The advantage of the IGIMF is that it acts as an overarching theory to previous attempts to explain puzzling observations in ETGs with ad-hoc variations of the IMF with their mass, their SFR, et cetera.

Whether Newtonian Dynamics or Milgromian dynamics is chosen is rather unimportant for high-luminosity ETGs, let alone which type of μ -function describes the transition from the quasi-Newtonian regime to the fully Milgromian regime correctly. This is because the luminous ETGs also have generally high accelerations at their half-mass radius. In principle, this reflects the fact that any theory of gravity must result in Newtonian gravity in every-day situations, independent of its behaviour with extremely low accelerations, like in galaxies.

Also this is in principle well known. Tortora et al. (2014) already discussed the observed σ_{obs} and M_{obs} in the

inner parts of 220 massive ETGs covered in the ATLAS^{3D}-survey (Cappellari et al. 2011) under the premise of Milgromian dynamics instead of non-baryonic dark matter. They found that also in Milgromian dynamics, the observed σ_{obs} and M_{obs} are better explained with a Salpeter IMF, i.e. an IMF that has (in contrast to the canonical IMF) a slope of $\alpha_1 = 2.3$ instead of $\alpha_1 = 1.3$. Samurović (2014) confirms this trend in a very detailed study of 10 massive ETGs, which appear too heavy to have formed with the canonical IMF, independent of whether Newtonian or Milgromian dynamics was chosen.

It is noteworthy that the dynamical masses are lower than the stellar masses for the majority of the ETGs with the highest stellar masses (see Fig. 10). This cannot be correct, because the dynamical mass of an ETG must encompass at least the mass of its stellar population. Thus, either the assumed star formation rates are too high for the most massive ETGs in our simple model, or these ETGs are the products of mergers of several smaller ETGs, for which $M_{\text{dyn}} > M_{\text{IGIMF}}$. This might also be in our simplified model, which only treats the dependence of IGIMF on the SFR for high stellar masses, but not its dependence on metallicity for low stellar masses. However, the dependence on metallicity likely plays a minor role compared to the dependence on the SFR for the M_{dyn}/L_V -ratios of the studied ETGs (see Section 3.2).

For low-acceleration ETGs in contrast, replacing Newtonian gravity with Milgromian gravity helps a great deal in explaining the apparent discrepancy between their expected accelerations based on their stellar populations mass and their observed dynamical mass based on their dynamics. However, also in Milgromian dynamics, the observed dynamical accelerations tend to be too high for the theoretical radial acceleration relations (RARs). On the other hand, the missing-mass problem is much smaller than for the Newtonian RAR. It even disappears in some low-acceleration ETGs, while not on averaging with windows that contain 21 ETGs.

The slight over-estimate of the average dynamical radial accelerations of the low-acceleration ETGs in Milgromian dynamics can especially be seen in Figs. 4, 6 and 8. These figures have the disadvantage that they neglect a possible rotation of the ETGs they show. The figures which do show an influence by rotation (Figs. 5, 7 and 9) encompass only a subset of the ETGs shown in the full sample, and predominantly the ETGs with low accelerations are missing because they are too faint, and thus challenging to observe. However, even if these low-acceleration ETGs would rotate, it would only increase the mass required to keep them bound, and the mismatch already seen in Figs. 4, 6 and 8 would become even larger.

This leads us to relax the assumption of virial equilibrium in the ETGs. For the high-luminosity ETGs, this is not an option, because they have also high radial accelerations and are therefore difficult to disturb from the outside. However, this may also be unnecessary for their dynamics, which could be explained by the IGIMF-theory. This is especially so, if the masses of the black holes they produced are rather high. This should not be a problem, because most stars, and thus also massive stars, probably formed in them when their metallicity was much lower than it is today (see figure 2 in Jeřábková et al. 2018). According to a comparison of fig-

ures 12 and 16 in Woosley et al. (2002), low-metallicity stars have higher masses when they become stellar-mass black holes.

The low-luminosity ETGs on the other hand also have low radial accelerations, especially if they do not contain dark matter (be it baryonic or non-baryonic), but only their stellar populations. They are therefore much easier to disturb. The magnitude of this disturbance can also be explained in Newtonian dynamics, as is shown by Kroupa (1997); Casas et al. (2012) and Domínguez et al. (2016). They could well reach mass-to-light ratios of $10^4 M_{\odot}/L_{\odot}$ during their long-lived remnant phase, if they are (then wrongly) assumed to be in virial equilibrium. Note that dynamical mass-to-light ratios and dynamical radial accelerations (e.g. equation 41) are both quantities that are linear in dynamical mass. Thus, raising the dynamical mass by a factor of, say, 10 would increase the dynamical radial acceleration and the dynamical mass-to-light ratio by the same amount. It is highly doubtful however, if this would concern *all* low-luminosity ETGs, like Newtonian dynamics implies in Figs. 4 to 9.

Milgromian dynamics on the other hand implies that some of them are probably disturbed by tidal fields, but not all of them, as can be seen in the same Figures. Also, the distortions would have to be less extreme than in Newtonian dynamics. The scenario of Milgromian dynamics appears to be more likely, if ETGs are indeed free of non-baryonic dark matter. This would have to be the case, if low-mass ETGs are indeed tidal dwarf galaxies, like their arrangement in disks of satellites suggests (Lynden-Bell 1976; Kroupa et al. 2005; Ibata et al. 2013; Ibata et al. 2014; Müller et al. 2016; Pawłowski & Kroupa 2020). This is because tidal dwarf galaxies do not contain non-baryonic dark matter, even if their progenitors did (Barnes & Hernquist 1992a; Bournaud 2010).

Thus, with all three ingredients together (i.e. the IGIMF, Milgromian dynamics and non-equilibrium dynamics), it may be possible to explain the dynamics of ETGs without dark matter. Without the IGIMF in particular, especially the dynamics of high-mass ETGs cannot be explained, as already noted in Dabringhausen et al. (2016) with the same ETGs. This is remedied in this paper by allowing the M_{dyn}/L_V -ratios of the massive ETGs to have a central peak, which is probably a consequence of the high star formation rates there in the past. This would have led to a top-heavy IMF in the past and more remnants today according to the IGIMF-model. Also rotation of the ETGs is discussed, in contrast to Dabringhausen et al. (2016). On the other hand, it is *not* the purpose of the present paper to offer exact solutions to the missing mass of individual ETGs, but rather to show that it can be found with well established alternatives to non-baryonic dark matter. The IGIMF-theory may be a key ingredient to finding the missing mass. However, further research is needed to fully understand the dynamics of ETGs. Notable is that by using the IGIMF-theory and Milgromian gravitation (MOND) to explain the M_{dyn}/L_V values, we confirm that more massive ETGs form more rapidly (downsizing). This is in turn consistent with ETGs having formed through direct free-fall collapse of non-rotating gas clouds (Eappen et al. 2022).

ACKNOWLEDGEMENTS

Jörg Dabringhausen and Pavel Kroupa acknowledge support from the Grant Agency of the Czech Republic under grant number 20-21855S. They also thank the Deutscher Akademischer Austauschdienst-Eastern European exchange program at the University of Bonn for supporting the Bonn-Prague exchange. Finally they acknowledge that particularly insightful suggestions by the anonymous referee improved the paper significantly. Throughout the preparation of this paper, they have made extensive use of NASA's Astrophysics Data System .

DATA AVAILABILITY

This paper utilizes the catalogue with the properties of early-type galaxies presented in Dabringhausen & Fellhauer (2016). No other data sources were used.

REFERENCES

- Abbott et al. 2016, *PhRvL*, 116, 061102
Ackermann et al. 2014, *PhRvD*, 89, 042001
Asencio E., Banik I., Mieske S., Venhola A., Kroupa P., Zhao H., 2022, *MNRAS*, 515, 2981
Bahcall J. N., 1984a, *ApJ*, 287, 926
Bahcall J. N., 1984b, *ApJ*, 276, 169
Banerjee S., Kroupa P., Oh S., 2012a, *ApJ*, 746, 15
Banerjee S., Kroupa P., Oh S., 2012b, *MNRAS*, 426, 1416
Banik I., Zhao H., 2021, arXiv e-prints, p. arXiv:2110.06936
Barnes J. E., Hernquist L., 1992a, *ARA&A*, 30, 705
Barnes J. E., Hernquist L., 1992b, *Nature*, 360, 715
Belokurov et al. 2006, *ApJ*, 647, L111
Belokurov et al. 2007, *ApJ*, 654, 897
Bender R., Burstein D., Faber S. M., 1992, *ApJ*, 399, 462
Bernardi M., Sheth R. K., Dominguez-Sanchez H., Fischer J. L., Chae K. H., Huertas-Company M., Shankar F., 2018, *MNRAS*, 477, 2560
Bertin G., Ciotti L., Del Principe M., 2002, *A&A*, 386, 149
Binney J., Tremaine S., 1987, *Galactic dynamics*. Princeton University Press
Blanchet L., Novak J., 2011, *MNRAS*, 412, 2530
Blanton M. R., Roweis S., 2007, *AJ*, 133, 734
Bolton A. S., Treu T., Koopmans L. V. E., Gavazzi R., Moustakas L. A., Bures S., Schlegel D. J., Wayth R., 2008, *ApJ*, 684, 248
Bosma A., 1981, *AJ*, 86, 1825
Bournaud F., 2010, *Advances in Astronomy*, 2010
Bournaud F., Duc P.-A., 2006, *A&A*, 456, 481
Bruzual G., Charlot S., 2003, *MNRAS*, 344, 1000
Bullock J. S., Boylan-Kolchin M., 2017, *ARA&A*, 55, 343
Candlish G. N., Smith R., Fellhauer M., 2015, *MNRAS*, 446, 1060
Caon N., Capaccioli M., D'Onofrio M., 1993, *MNRAS*, 265, 1013
Cappellari et al. 2006, *MNRAS*, 366, 1126
Cappellari et al. 2011, *MNRAS*, 413, 813
Cappellari et al. 2012, *Nature*, 484, 485
Cappellari et al. 2013a, *MNRAS*, 432, 1709
Cappellari et al. 2013b, *MNRAS*, 432, 1862
Casas R. A., Arias V., Peña Ramírez K., Kroupa P., 2012, *MNRAS*, 424, 1941
Chabrier G., 2003, *PASP*, 115, 763
Chae K.-H., 2022, *ApJ*, 941, 55
Chae K.-H., Bernardi M., Sheth R. K., 2018, *ApJ*, 860, 81
Chae K.-H., Bernardi M., Sheth R. K., 2019, *ApJ*, 874, 41
Chae K.-H., Bernardi M., Sheth R. K., Gong I.-T., 2019, *ApJ*, 877, 18
Chae K.-H., Desmond H., Lelli F., McGaugh S. S., Schombert J. M., 2021, *ApJ*, 921, 104
Chae K.-H., Lelli F., Desmond H., McGaugh S. S., Li P., Schombert J. M., 2020, *ApJ*, 904, 51
Ciotti L., 1991, *A&A*, 249, 99
Clark G. W., 1975, *ApJ*, 199, L143
Crowther P. A., Schnurr O., Hirschi R., Yusof N., Parker R. J., Goodwin S. P., Kassim H. A., 2010, *MNRAS*, 408, 731
Dabringhausen J., 2019, *MNRAS*, 490, 848
Dabringhausen J., Fellhauer M., 2016, *MNRAS*, 460, 4492
Dabringhausen J., Hilker M., Kroupa P., 2008, *MNRAS*, 386, 864
Dabringhausen J., Kroupa P., 2013, *MNRAS*, 429, 1858
Dabringhausen J., Kroupa P., Baumgardt H., 2009, *MNRAS*, 394, 1529
Dabringhausen J., Kroupa P., Famaey B., Fellhauer M., 2016, *MNRAS*, 463, 1865
Dabringhausen J., Kroupa P., Pflamm-Altenburg J., Mieske S., 2012, *ApJ*, 747, 72
Dariush et al. 2016, *MNRAS*, 456, 2221
de La Rosa I. G., La Barbera F., Ferreras I., de Carvalho R. R., 2011, *MNRAS*, 418, L74
De Lucia G., Blaizot J., 2007, *MNRAS*, 375, 2
de Vaucouleurs G., de Vaucouleurs A., Corwin Herold G. J., Buta R. J., Paturel G., Fouque P., 1991, *Third Reference Catalogue of Bright Galaxies*
Deason A. J., Belokurov V., Evans N. W., Watkins L. L., Fellhauer M., 2012, *MNRAS*, 425, L101
Del Popolo A., Le Delliou M., 2017, *Galaxies*, 5, 17
Demircan O., Kahraman G., 1991, *Ap&SS*, 181, 313
Domínguez R., Fellhauer M., Blaña M., Farias J. P., Dabringhausen J., Candlish G. N., Smith R., Choque N., 2016, *MNRAS*, 461, 3630
Domínguez Sánchez H., Bernardi M., Brownstein J. R., Drory N., Sheth R. K., 2019, *MNRAS*, 489, 5612
Duc P.-A., Bournaud F., Masset F., 2004, *A&A*, 427, 803
Duquenois A., Mayor M., 1991, *A&A*, 248, 485
Eappen R., Kroupa P., Wittenburg N., Haslbauer M., Famaey B., 2022, *MNRAS*, 516, 1081
Einstein A., 1916, *Annalen der Physik*, 354, 769
Famaey B., Binney J., 2005, *MNRAS*, 363, 603
Famaey B., McGaugh S. S., 2012, *Living Reviews in Relativity*, 15, 10
Fellhauer M., Kroupa P., 2006, *MNRAS*, 367, 1577
Ferreras I., La Barbera F., de la Rosa I. G., Vazdekis A., de Carvalho R. R., Falcón-Barroso J., Ricciardelli E., 2013, *MNRAS*, 429, L15
Fontanot F., De Lucia G., Hirschmann M., Bruzual G., Charlot S., Zibetti S., 2017, *MNRAS*, 464, 3812
Forbes D. A., Kroupa P., 2011, *PASA*, 28, 77
Forbes D. A., Lasky P., Graham A. W., Spitler L., 2008, *MNRAS*, 389, 1924

- Gao L., White S. D. M., Jenkins A., Stoeckl F., Springel V., 2004, *MNRAS*, 355, 819
- Geha M., Guhathakurta P., van der Marel R. P., 2003, *AJ*, 126, 1794
- Gentile G., Famaey B., de Blok W. J. G., 2011, *A&A*, 527, A76
- Gieles M., Baumgardt H., Heggie D. C., Lamers H. J. G. L. M., 2010, *MNRAS*, 408, L16
- Graham A., Colless M., 1997, *MNRAS*, 287, 221
- Gu M., Greene J. E., Newman A. B., Kreisch C., Quenneville M. E., Ma C.-P., Blakeslee J. P., 2022, *ApJ*, 932, 103
- Gunawardhana et al. 2011, *MNRAS*, 415, 1647
- Haghi H., Bazkiaei A. E., Zonoozi A. H., Kroupa P., 2016, *MNRAS*, 458, 4172
- Hammer F., Yang Y., Fouquet S., Pawlowski M. S., Kroupa P., Puech M., Flores H., Wang J., 2013, *MNRAS*
- Haslbauer M., Dabringhausen J., Kroupa P., Javanmardi B., Banik I., 2019, *A&A*, 626, A47
- Hees A., Famaey B., Angus G. W., Gentile G., 2016, *MNRAS*, 455, 449
- Ibata N. G., Ibata R. A., Famaey B., Lewis G. F., 2014, *Nature*, 511, 563
- Ibata R. A., Famaey B., Lewis G. F., Ibata N. G., Martin N., 2015, *ApJ*, 805, 67
- Ibata et al. 2013, *Nature*, 493, 62
- Ivanova N., Heinke C. O., Rasio F. A., Belczynski K., Fregeau J. M., 2008, *MNRAS*, 386, 553
- Janz J., Cappellari M., Romanowsky A. J., Ciotti L., Alabi A., Forbes D. A., 2016, *MNRAS*, 461, 2367
- Javanmardi B., Martinez-Delgado D., Kroupa P., Henkel C., Crawford K., Teuwen K., Gabany R. J., Hanson M., Chonis T. S., Neyer F., 2016, *A&A*, 588, A89
- Jeřábková T., Hasani Zonoozi A., Kroupa P., Beccari G., Yan Z., Vazdekis A., Zhang Z. Y., 2018, *A&A*, 620, A39
- Kalirai J. S., Hansen B. M. S., Kelson D. D., Reitzel D. B., Rich R. M., Richer H. B., 2008, *ApJ*, 676, 594
- King I., 1962, *AJ*, 67, 471
- Kroupa P., 1995, *MNRAS*, 277, 1491
- Kroupa P., 1997, *New Astronomy*, 2, 139
- Kroupa P., 2001, *MNRAS*, 322, 231
- Kroupa P., 2002, *Science*, 295, 82
- Kroupa P., Gilmore G. F., 1994, *MNRAS*, 269, 655
- Kroupa P., Jerabkova T., Thies I., Pflamm-Altenburg J., Famaey B., Boffin H. M. J., Dabringhausen J., Beccari G., Prusti T., Boily C., Haghi H., Wu X., Haas J., Zonoozi A. H., Thomas G., Šubr L., Aarseth S. J., 2022, *MNRAS*, 517, 3613
- Kroupa P., Theis C., Boily C. M., 2005, *A&A*, 431, 517
- Kroupa P., Weidner C., 2003, *ApJ*, 598, 1076
- Kroupa P., Weidner C., Pflamm-Altenburg J., Thies I., Dabringhausen J., Marks M., Maschberger T., 2013, *The Stellar and Sub-Stellar Initial Mass Function of Simple and Composite Populations*. p. 115
- Kroupa et al. 2010, *A&A*, 523, 32
- La Barbera F., Ferreras I., Vazdekis A., de la Rosa I. G., de Carvalho R. R., Trevisan M., Falcón-Barroso J., Ricciardelli E., 2013, *MNRAS*, 433, 3017
- La Barbera F., Vazdekis A., Ferreras I., Pasquali A., Alende Prieto C., Martín-Navarro I., Aguado D. S., de Carvalho R. R., Rembold S., Falcón-Barroso J., van de Ven G., 2019, *MNRAS*, 489, 4090
- La Barbera F., Vazdekis A., Ferreras I., Pasquali A., Cappellari M., Martín-Navarro I., Schönebeck F., Falcón-Barroso J., 2016, *MNRAS*, 457, 1468
- Lee et al. 2009, *ApJ*, 706, 599
- Leier D., Ferreras I., Saha P., Charlot S., Bruzual G., La Barbera F., 2016, *MNRAS*
- Lelli F., McGaugh S. S., Schombert J. M., Pawlowski M. S., 2017, *ApJ*, 836, 152
- Li Y.-S., De Lucia G., Helmi A., 2010, *MNRAS*, 401, 2036
- Lüghausen F., Famaey B., Kroupa P., 2015, *Canadian Journal of Physics*, 93, 232
- Lynden-Bell D., 1976, *MNRAS*, 174, 695
- Marks M., Kroupa P., 2011, *MNRAS*, 417, 1702
- Marks M., Kroupa P., Dabringhausen J., Pawlowski M. S., 2012, *MNRAS*, 422, 2246
- Mateo M. L., 1998, *ARA&A*, 36, 435
- Matteucci F., Recchi S., 2001, *ApJ*, 558, 351
- McConnachie A. W., 2012, *AJ*, 144, 4
- McDermid R. M., Alatalo K., Blitz L. e. a., 2015, *MNRAS*, 448, 3484
- McGaugh S. S., 2008, *ApJ*, 683, 137
- McGaugh S. S., Lelli F., Schombert J. M., 2016, *PhRvL*, 117, 201101
- McGaugh S. S., Wolf J., 2010, *ApJ*, 722, 248
- Metz M., Kroupa P., 2007, *MNRAS*, 376, 387
- Metz M., Kroupa P., Libeskind N. I., 2008, *ApJ*, 680, 287
- Milgrom M., 1983a, *ApJ*, 270, 371
- Milgrom M., 1983b, *ApJ*, 270, 365
- Milgrom M., 2012, *Physical Review Letters*, 109, 131101
- Misgeld I., Hilker M., 2011, *MNRAS*, 414, 3699
- Misgeld I., Hilker M., Mieske S., 2009, *A&A*, 496, 683
- Misgeld I., Mieske S., Hilker M., 2008, *A&A*, 486, 697
- Moore B., Governato F., Quinn T., Stadel J., Lake G., 1998, *ApJ*, 499, L5
- Muñoz R. R., Geha M., Willman B., 2010, *AJ*, 140, 138
- Müller O., Jerjen H., Pawlowski M. S., Binggeli B., 2016, *A&A*, 595, A119
- Müller O., Pawlowski M. S., Jerjen H., Lelli F., 2018, *Science*, 359, 534
- Müller O., Pawlowski M. S., Lelli F., Fahrion K., Rejkuba M., Hilker M., Kanehisa J., Libeskind N., Jerjen H., 2021, *A&A*, 645, L5
- Navarro J. F., Frenk C. S., White S. D. M., 1996, *ApJ*, 462, 563
- Oey M. S., Clarke C. J., 2005, *ApJ*, 620, 43
- Okazaki T., Taniguchi Y., 2000, *ApJ*, 543, 149
- Parikh et al. 2018, *MNRAS*, 477, 3954
- Patel E., Kallivayalil N., Garavito-Camargo N., Besla G., Weisz D. R., van der Marel R. P., Boylan-Kolchin M., Pawlowski M. S., Gómez F. A., 2020, *ApJ*, 893, 121
- Pawlowski M. S., 2018, *Modern Physics Letters A*, 33, 1830004
- Pawlowski M. S., Kroupa P., 2020, *MNRAS*, 491, 3042
- Pawlowski M. S., Kroupa P., Angus G., de Boer K. S., Famaey B., Hensler G., 2012, *MNRAS*, 424, 80
- Pawlowski M. S., Kroupa P., Jerjen H., 2013, *MNRAS*, 435, 1928
- Pawlowski M. S., McGaugh S. S., Jerjen H., 2015, *MNRAS*, 453, 1047
- Pawlowski M. S., Pflamm-Altenburg J., Kroupa P., 2012, *MNRAS*, p. 2990
- Pawlowski M. S., Tony Sohn S., 2021, *ApJ*, 923, 42

- Pawlowski et al. 2014, MNRAS, 442, 2362
- Perivolaropoulos L., Skara F., 2021, arXiv e-prints, p. arXiv:2105.05208
- Pflamm-Altenburg J., Weidner C., Kroupa P., 2007, ApJ, 671, 1550
- Planck Collaboration et al. 2020, A&A, 641, A6
- Plummer H. C., 1911, MNRAS, 71, 460
- Raghavan D., McAlister H. A., Henry T. J., Latham D. W., Marcy G. W., Mason B. D., Gies D. R., White R. J., ten Brummelaar T. A., 2010, ApJS, 190, 1
- Recchi S., Calura F., Kroupa P., 2009, A&A, 499, 711
- Romano D., Matteucci F., Zhang Z. Y., Papadopoulos P. P., Ivison R. J., 2017, MNRAS, 470, 401
- Rubin V. C., Burstein D., Ford W. K. J., Thonnard N., 1985, ApJ, 289, 81
- Rubin V. C., Ford W. K. J., Thonnard N., 1978, ApJ, 225, L107
- Ryan-Weber E. V., Begum A., Oosterloo T., Pal S., Irwin M. J., Belokurov V., Evans N. W., Zucker D. B., 2008, MNRAS, 384, 535
- Samurović S., 2014, A&A, 570, A132
- Sarzi M., Spiniello C., La Barbera F., Krajnović D., van den Bosch R., 2018, MNRAS, 478, 4084
- Scodreggio M., Giovanelli R., Haynes M. P., 1998, AJ, 116, 2738
- Sérsic J. L., 1963, Boletín de la Asociación Argentina de Astronomía La Plata Argentina, 6, 41
- Sersic J. L., 1968, Atlas de Galaxias Australes
- Smith R. J., 2020, ARA&A, 58, 577
- Smith et al. 2015, MNRAS, 454, 2502
- Strigari L. E., Bullock J. S., Kaplinghat M., Simon J. D., Geha M., Willman B., Walker M. G., 2008, Nature, 454, 1096
- Teyssier R., 2002, A&A, 385, 337
- Thomas D., Maraston C., Bender R., Mendes de Oliveira C., 2005, ApJ, 621, 673
- Thorsett S. E., Chakrabarty D., 1999, ApJ, 512, 288
- Toomre A., 1977, in B. M. Tinsley & R. B. Larson ed., Evolution of Galaxies and Stellar Populations Mergers and Some Consequences. pp 401–+
- Tortora C., Napolitano N. R., Romanowsky A. J., Capaccioli M., Covone G., 2009, MNRAS, 396, 1132
- Tortora C., Romanowsky A. J., Cardone V. F., Napolitano N. R., Jetzer P., 2014, MNRAS, 438, L46
- van Dokkum P., Conroy C., Villaume A., Brodie J., Romanowsky A. J., 2017, ApJ, 841, 68
- van Dokkum P. G., Conroy C., 2010, Nature, 468, 940
- Vudragović A., Samurović S., Jovanović M., 2016, A&A, 593, A40
- Walker M. G., Belokurov V., Evans N. W., Irwin M. J., Mateo M., Olszewski E. W., Gilmore G., 2009, ApJ, 694, L144
- Weidner C., Ferreras I., Vazdekis A., La Barbera F., 2013, MNRAS, 435, 2274
- Weidner C., Kroupa P., 2004, MNRAS, 348, 187
- Weidner C., Kroupa P., Bonnell I. A. D., 2010, MNRAS, 401, 275
- Weidner C., Kroupa P., Larsen S. S., 2004, MNRAS, 350, 1503
- Weidner C., Kroupa P., Pflamm-Altenburg J., 2011, MNRAS, pp 979–86
- Weidner C., Kroupa P., Pflamm-Altenburg J., Vazdekis A., 2013, MNRAS, 436, 3309
- Weisz D. R., Dolphin A. E., Skillman E. D., Holtzman J., Gilbert K. M., Dalcanton J. J., Williams B. F., 2014, ApJ, 789, 148
- Willman B., Geha M., Strader J., Strigari L. E., Simon J. D., Kirby E., Ho N., Warres A., 2011, AJ, 142, 128
- Wolf J., Martinez G. D., Bullock J. S., Kaplinghat M., Geha M., Muñoz R. R., Simon J. D., Avedo F. F., 2010, MNRAS, 406, 1220
- Woosley S. E., Heger A., Weaver T. A., 2002, Reviews of Modern Physics, 74, 1015
- Worthey G., 1994, ApJS, 95, 107
- Wu X., Kroupa P., 2015, MNRAS, 446, 330
- Yan Z., Jerabkova T., Kroupa P., 2017, A&A, 607, A126
- Yan Z., Jerabkova T., Kroupa P., 2020, A&A, 637, A68
- Yan Z., Jerabkova T., Kroupa P., Vazdekis A., 2019a, A&A, 629, A93
- Yan Z., Jerabkova T., Kroupa P., Vazdekis A., 2019b, A&A, 629, A93
- Yan Z., Jeřábková T., Kroupa P., 2021, A&A, 655, A19
- Yang Y., Hammer F., Fouquet S., Flores H., Puech M., Pawlowski M. S., Kroupa P., 2014, MNRAS, 442, 2419
- Young et al. 2011, MNRAS, 414, 940
- Zhang Z.-Y., Romano D., Ivison R. J., Papadopoulos P. P., Matteucci F., 2018, Nature, 558, 260
- Zhao H. S., Famaey B., 2006, ApJ, 638, L9

APPENDIX

For comparison with Figs. 6 to 9 in the main paper, Fig 12 shows the more extreme choice made by van Dokkum et al. (2017) for the dependency of the mass-to-light ratio with the radius of the ETGs (i.e. $\epsilon = 2.33$ and $\eta = 6.0$ instead of $\epsilon = 1.29$ and $\eta = 3.33$ in equation 21). In this figure, the ETGs are assumed to rotate and to have black holes from metal-rich massive stars. Thus, the assumptions are identical to the ones in Fig. 7, except for the relation describing the change of the mass-to-light ratio with radius. Consequently, even more ETGs have $M_{\text{dyn}} < M_{\text{IGIMF}}$ in this figure than in fig. 7. Thus, the finding of Chae et al. (2018) and Domínguez Sánchez et al. (2019) that the standard case is more probable than the extreme case is corroborated here by using IGIMF-based stellar population synthesis.

with IGIMF, light BHs, with rotation and with binaries

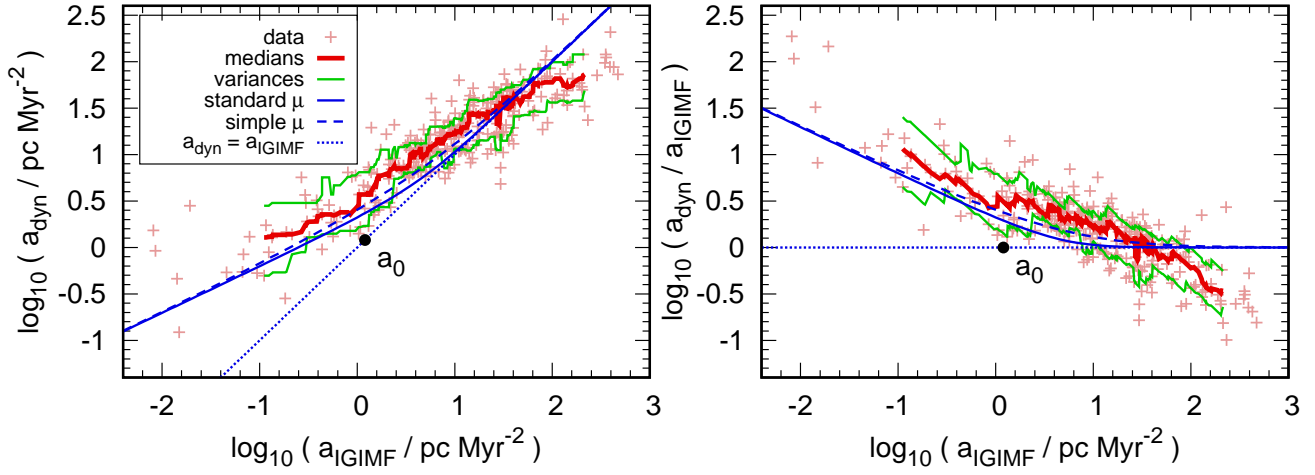


Figure 12. As Fig. 7, but with the higher increase in stellar mass resulting from the more extreme parameters $\epsilon = 2.33$ and $\eta = 6.0$ in equation 21 from van Dokkum et al. (2017), rather than the standard case ($\epsilon = 1.29$ and $\eta = 3.33$) from Bernardi et al. (2018).